united nations
educational, scientific
and cultural
organization

international atomic
energy agency

the
abdus salam
international centre for theoretical physics

H4.SMR/1330-23

" Sixth Workshop on Non-Linear Dynamics and Earthquake Prediction"

15 - 27 October 2001

A Continuum Approach to Friction and Brittle Instability

A. Agnon

Institute of Earth Sciences
The Hebrew University
Jerusalem

JOURNAL OF GEOPHYSICAL RESEARCH, VOL. 102, NO. B12, PAGES 27,635–27,649, DECEMBER 10, 1997

Distributed damage, faulting, and friction

Vladimir Lyakhovsky
Institute of Earth Sciences, The Hebrew University, Jerusalem

Yehuda Ben-Zion
Department of Earth Sciences, University of Southern California, Los Angeles

Amotz Agnon
Institute of Earth Sciences, The Hebrew University, Jerusalem

Abstract. We present a formulation for mechanical modeling of geological processes in the seismogenic crust using damage rheology. The seismogenic layer is treated as an elastic medium where distributed damage, modifying the elastic stiffness, evolves as a function of the deformation history. The model damage rheology is based on thermodynamic principles and fundamental observations of rock deformation. The theoretical analysis leads to a kinetic equation for damage evolution having two principal coefficients. The first is a criterion for the transition between strength degradation and recovering (healing), and is related to friction. The second is a rate coefficient of damage evolution which can have different values or functional forms for positive (degradation) and negative (healing) evolution. We constrain these coefficients by fitting model predictions to laboratory data, including coefficient of friction in sawcut setting, intact strength in fracture experiments, first yielding in faulting experiments under three-dimensional strain, onset and evolution of acoustic emission, and dynamic instability. The model damage rheology accounts for many realistic features of three-dimensional deformation fields associated with an earthquake cycle. These include aseismic deformation, gradual strength degradation, development of process zones and branching faults around high-damage areas, strain localization, brittle failure, and state dependent friction. Some properties of the model damage rheology (e.g., cyclic stick-slip behavior with possible accompanying creep) are illustrated with simplified analytical results. The developments of the paper provide an internally consistent framework for simulating long histories of crustal deformation, and studying the coupled evolution of regional earthquakes and faults. This is done in a follow up work.

1. Introduction

Rocks exhibit a wide variety of rheological behaviors ranging from viscoelastic deformation to plastic flow and localized faulting. A great challenge of theoretical geodynamic studies is to incorporate multi rheological behavior, including faulting, into models that simulate deformational processes in the upper crust. At the present time, a generally accepted method for describing time-dependent deformational processes in the brittle-elastic parts of the lithosphere is not available. The purpose of this paper and a follow-up work (*V. Lyakhovsky, Y. Ben-Zion, and A. Agnon, manuscript in preparation*; herein after referred to as paper 2) is to develop a useful framework for studies concerned with seismic and aseismic deformations in large domains of space and time. The overall large-scale structure of our model is a layered elastic-viscoelastic half-space incorporating damage rheology. In the present paper we focus on theory and observations relevant to the damage rheology and its coupling with viscous relaxation. In paper 2 we discuss the other components of the model and provide various simulation examples.

Paper number 97JB01896.
0148-0227/97/97JB-01896$09.00

Brittle behavior is often modeled by a rigid elastic-plastic solid that is governed by simple static-kinetic friction or Byerlee's law [*Brace and Kohlstedt*, 1980]. However, such models do not account for details of strength evolution and they thus cannot be used to study important portions of the deformation field, such as nucleation of slip instabilities. The rate- and state-dependent (RS) friction model [e.g., *Dieterich*, 1979, 1981; *Ruina*, 1983] provides a framework that can be used to simulate all important aspects of an earthquake cycle, including stable slip, nucleation of instabilities, rupture propagation, and healing. However, the RS formulation assumes that deformation at all stages occurs on well defined frictional surfaces, and it does not provide a mechanism for understanding distributed deformation. In addition, it is not clear [e.g., *Andrews*, 1989; *Ben-Zion and Rice*, 1995] to what extent the existing RS friction laws are valid for natural conditions involving complex geometry, large values of slip, slip rate, and time, etc.

Various simple conceptual schemes based on a network of blocks and springs [e.g., *Burridge and Knopoff*, 1967; *Carlson and Langer*, 1989] have been used to simulate static, quasi-static, and dynamic sliding processes. *Rice* [1993] and *Ben-Zion* and *Rice* [1993, 1995] criticized the validity of representing a fault in elastic solid with a block-spring array. They simulated slip histories on various types of a two-

dimensional (2-D) strike-slip fault in a 3-D elastic half-space with models incorporating continuum elasticity. *Cowie et al.* [1993], *Sornette et al.* [1994], and *Ward* [1996] simulated the development of fault patterns and regional earthquakes in 2-D elastic solids: we discuss these models in more detail in paper 2. *Lockner and Madden* [1991 a, b] developed a numerical multiple-crack model for the failure process of a brittle solid which simulates growth of microcracks on a regular array of potential crack sites. This and similar numerical models reproduce various common features of fracturing processes, especially those occurring in some fabricated materials, but they cannot explain fault patterns observed in experiments [e.g., *Reches*, 1988] or in the field [e.g., *Segall and Pollard*, 1983]. Fracture distributions in situ and fragmentation of rocks in laboratory samples show fractal-like patterns [e.g., *King*, 1983; *Turcotte*, 1986; *Okubo and Aki*, 1987; *Aviles et al.*, 1987]. Thus fracture network simulations should not depend on specific length scales, such as length scales prescribed in regular arrays.

A rheological model of the faulting process should include subcritical crack growth from very early stages of the loading, material degradation due to increasing crack concentration, macroscopic brittle failure, post failure deformation, and healing. Suitable variables should be defined to characterize the above deformational aspects quantitatively in a framework compatible with continuum mechanics and thermodynamics. Among such approaches are *Robinson*'s [1952] linear cumulative creep damage law, *Hoff*'s [1953] ductile creep rupture theory, *Kachanov*'s [1958, 1986] brittle rupture theory, *Rabotnov*'s [1969, 1988] coupled damage creep theory, and many modifications of these theories. Several researchers (see the review of *Kachanov*, [1994]) proposed models with a scalar damage parameter changing from 0 at an undamaged state to 1 at failure. The scalar damage models fit reasonably well existing experimental results, including culmination of damage in concrete subjected to fatigue loading [*Papa*, 1993] and damage increase in 2024-T3 aluminum alloy under different loading and temperature conditions [*Hansen and Schreyer*, 1994]. In the study of *Hansen and Schreyer* [1994], the scalar isotropic damage model correlates with all measured quantities except the change in the apparent Poisson ratio. For this reason, *Ju* [1990] and *Hansen and Schreyer* [1994] suggested upgrading the damage parameter from a scalar to tensor quantity. Such an anisotropic tensorial damage model contains at least three adjustable parameters which permit correct simulation of the apparent Poisson ratio.

Variations of elastic moduli and Poisson's ratio with extent of damage, under different types of load, can also be described using a nonlinear elastic model with scalar damage provided that it is scaled properly with the ratio of strain invariants. This has been done in the damage model proposed by *Lyakhovsky and Myasnikov* [1984, 1985], *Myasnikov et al.* [1990], and *Lyakhovsky et al.* [1993]. Previous applications of this model to geodynamic problems were given by *Ben-Avraham and Lyakhovsky* [1992], *Lyakhovsky et al.* [1994], and *Agnon and Lyakhovsky* [1995]. The scalar damage model accurately reproduces results from the four point beam test [*Lyakhovsky et al.*, 1997]. Here we provide additional developments of the above model, and constrain the final model parameters by comparisons of theoretical predictions with various laboratory results. In paper 2 we incorporate the damage rheology into a model of a 3-D layered half-space and provide examples of simulated patterns of seismicity and faulting.

2. Distributed Damage in Rocks

We briefly list below some indications of damage in natural rocks and rock samples which form the observational basis for our theoretical damage model for the crust. Pioneering studies of fractures and faults treated the crust as an infinite, perfectly elastic medium [e.g., *Anderson*, 1951]. Subsequent studies accounted for the finite length of faults, and the perturbation to the regional stress field due to the proximity of additional faults [*Chinnery*, 1966 a, b]. Field mapping often shows that the density of faults depends on the scale of the map, so higher resolution increases the number of faults in a given domain [*Scholz*, 1990]. This complexity limits the use of methods that specify the positions of isolated cracks in the deforming region.

Classical fracture mechanics postulates that in a linear elastic solid an isolated crack will propagate at velocities approaching the speed of sound in the medium once a critical stress intensity factor K_c has been reached or exceeded at the crack tip [*Irwin*, 1958]. At lower stress intensity factors the crack remains stable. A more general approach in classical fracture mechanics is to consider the strain energy release rate G during crack extension [e.g., *Freund*, 1990]. Dynamic crack extension occurs when G reaches a critical value G_c.

These fracture mechanics approaches have been used successfully to predict catastrophic crack propagation in metals, ceramics, and glasses. In grainy materials, however, the stress field is highly nonuniform on the grain scale. Stress intensity factors K and strain energy release rates G are calculated macroscopically, neglecting stress concentrations due to grain contacts and energy release due to intergranular sliding. Such materials subjected to long-term loading show significant rates of macroscopic crack extension at values of K and G significantly lower than the critical. This phenomenon is known as subcritical crack growth [*Swanson*, 1984, *Atkinson and Meredith*, 1987; *Cox and Scholz*, 1988].

The investigations of granite fracturing by *Yukutake* [1989], *Lockner et al.* [1991], and *Reches and Lockner* [1994] show that fracturing cannot be described in terms of propagation of a single crack. Several experimental studies revealed that elastic parameters strongly depend on the deformational history (i.e., damage extent), leading to vanishing elastic moduli at large stresses just before failure [*Lockner and Byerlee*, 1980]. While linear elastic fracture mechanics assumes the size of the inelastic zone at the crack tip to be negligibly small, the experiments show that this zone has a significant size.

In most engineering and rock-like materials a slowly propagating crack is preceded by an evolving damage zone distributed around its tip [e.g., *Bazant and Cedolin*, 1991; *Lockner et al.*, 1991]. The distributed damage modifies the elastic coefficients in the medium around the tip and hence controls the macrocrack trajectory and the growth rate [*Huang et al.*, 1991; *Chai*, 1993]. The finite size effect of the fracture process zone is often treated with models which specify a cohesive zone near the crack tip within the plane of the crack [*Dugdale*, 1960; *Barenblatt*, 1962; *Ida*, 1972; *Palmer and Rice*, 1973, *Rubin*, 1995 a, b]. This approach is useful when the crack geometry is well defined, and in contrast to linear elastic fracture mechanics, the cohesion zone models do not contain an unphysical crack tip singularity.

Field observations suggest that the size of the damage zone (or process zone) grows with the size of the fracture, in viola-

tion of the premises of the critical stress intensity factor approach [*Rubin*, 1995 a, b]. This is decisively documented around dikes that form by the injection of magma into fractures [*Delaney et al.*, 1986; *Baer*, 1991; *Weinberger et al.*, 1995; *Hoek*, 1995], and is also compatible with results of *Papageorgiou and Aki* [1983] who inverted seismic strong motion data for earthquake source parameters in the context of their specific barrier model. An early theoretical discussion of this phenomenon is given by *Andrews* [1976].

Andrews and Ben-Zion [1997] showed that earthquake rupture can propagate along an interface separating different elastic media in a wrinkle-like mode associated with little loss of energy to friction. Thus it is energetically favorable for ruptures to be located along the material interface between the gouge and the surrounding rock, rather than within the gouge. In such circumstances the damage zones of successive earthquake ruptures continue to create fresh gouge material, thus adding to the overall thickness of the (damaged) fault zone. This may help to explain field and laboratory correlations [e.g., *Hull*, 1988; *Robertson*, 1983] between gouge thickness and cumulative number of earthquakes (or slip) along the fault.

It is important to consider an additional property of rocks when choosing a rheology for simulations of earthquake cycles. Experimental studies of rock deformation [e.g., *Nishihara*, 1957; *Ambartsumyan*, 1982; *Weinberger et al.*, 1994] reveal a strong dependence of elastic coefficients on the type of loading, which results in abrupt changes of the elastic moduli when the loading reverses from tension to compression. Abrupt changes of elastic properties are commonly observed in grainy materials. For example, the tensile Young modulus of graphite is 20% less than the compressive one [*Jones*, 1977]. Jumps of Young moduli can be 30% for different types of iron, and in concrete the compressive modulus may be up to 3 times larger than the tensile one [*Ambartsumyan*, 1982]. Results of various experiments with Westerly granite, marble, diabase, and weak granite from Kola Peninsula, compiled by *Lyakhovsky* [1990] and *Lyakhovsky et al.* [1993], show high sensitivity of rock elasticity to the type of loading.

It is reasonable to assume that the extent of the latter nonlinearity in the elastic response of rocks depends strongly on the state of damage. Perfectly intact and undamaged rock should not display nonlinear elasticity for small strains. On the other hand, a rock that is highly damaged along a plane can respond to uniaxial extension normal to the damage plane with small elastic stress, whereas it will respond to uniaxial compression in a manner similar to intact rock.

In the following sections we first discuss the thermodynamics of damage growth in elastic solid. Then we construct a phenomenological model that relates damage to the elastic response in an internally consistent manner. Finally, we constrain the obtained model parameters by comparisons of theoretical predictions with experimental results.

3. Model of Medium With Distributed Damage

3.1. General Thermodynamic Formulation

Here we present the construction of a new rheological model accounting for elastic deformation, viscous relaxation, and evolution of damage (material degradation as well as healing). We follow the approach of irreversible thermodynamics [*Onsager*, 1931; *Prigogine*, 1955; *deGroot and Mazur*, 1962], which was successfully applied to kinetics of chemical reactions and phase transitions [e.g., *Fitts*, 1962; *deGroot and Mazur*, 1962] and as a basis for variational methods of continuous media models [e.g., *Sedov*, 1968; *Malvern*, 1969]. Following this framework, *Mosolov and Myasnikov* [1965] first formulated a variational approach to the model of viscoplastic media [see also *Ekland and Temam*, 1976]. *Lyakhovsky and Myasnikov* [1985] first used the balance equations of energy and entropy to establish a thermodynamical foundation for a rheological model of damaged material [*Myasnikov et al.*, 1990; *Lyakhovsky et al.*, 1993]. A similar approach was later used as the basis of other damage models [e.g., *Valanis*, 1990; *Hansen and Schreyer*, 1994].

Many workers in continuum thermodynamics have postulated that the free energy density is a function of various state variables, including "hidden variables" [*Coleman and Gurtin*, 1967; *Lubliner*, 1972] not available for macroscopic observation. In order to simulate a process of fracturing in terms of continuum mechanics, a nondimensional intensive damage variable α is introduced. The variable α can be envisioned as the density of microcracks in a laboratory specimen, or as the density of small faults in a crustal domain. The free energy of a solid, F, is assumed to be given by

$$F = F(T, \varepsilon_{ij}, \alpha), \tag{1}$$

where T and ε_{ij} are the macroscopic temperature and Cauchy tensor of infinitesimal elastic deformation, respectively, and α is a nondimensional damage state variable. The elastic strain tensor ε_{ij} is written as the difference between a current metric tensor g_{ij} and a metric tensor describing the irreversible deformation, g^0_{ij}:

$$\varepsilon_{ij} = g_{ij} - g^0_{ij}. \tag{2}$$

It may be represented through small elastic displacements u_i,

$$\varepsilon_{ij} = \frac{1}{2}\left(\frac{\partial u_i}{\partial x_j} + \frac{\partial u_j}{\partial x_i}\right). \tag{3}$$

The strain rate tensor is given as a temporal derivative of the current metric tensor

$$e_{ij} = \frac{dg_{ij}}{dt}. \tag{4}$$

The balance equations of the internal energy U and entropy S accounting for irreversible changes of viscous deformation and material damage [e.g., *Malvern*, 1969] have the form

$$\frac{dU}{dt} = \frac{d}{dt}(F + TS) = \frac{1}{\rho}\left(\sigma_{ij}e_{ij} - \nabla_i J_i\right), \tag{5}$$

$$\frac{dS}{dt} = -\nabla_i\left(\frac{J_i}{T}\right) + \Gamma, \tag{6}$$

where ρ is mass density. Here J_i is heat flux and Γ is local entropy production. Both J_i and Γ result from dissipative irreversible processes such as internal friction and creation of new surfaces. Substituting (5) into (6) and using an equation for production of free energy [e.g., *Gibbs*, 1961]

$$dF = -SdT + \frac{\partial F}{\partial \varepsilon_{ij}} d\varepsilon_{ij} + \frac{\partial F}{\partial \alpha} d\alpha, \tag{7}$$

and the definition of the Cauchy stress tensor

$$\sigma_{ij} = \rho \frac{\partial F}{\partial \varepsilon_{ij}}, \tag{8}$$

the local entropy production may be represented as

$$\Gamma = -\frac{J_i}{\rho T^2}\nabla_i T + \frac{1}{\rho T}\sigma_{ij}\frac{dg^0_{ij}}{dt} - \frac{1}{T}\frac{\partial F}{\partial \alpha}\frac{d\alpha}{dt}. \tag{9a}$$

The first term of equation (9a) describes entropy production by heat conduction, the second term is due to dissipation for a viscous flow, and the third term is related to the damage process. We neglect heat production by radioactive decay and chemical processes. These processes are independent to first order; hence, as is commonly assumed, each term in (9a) must be positive. The part of the entropy production related to the damage process, Γ_α, is

$$\Gamma_\alpha = -\frac{1}{T}\frac{\partial F}{\partial \alpha}\frac{d\alpha}{dt}. \tag{9b}$$

We expand Γ_α as a Taylor series with respect to $d\alpha/dt$ around an equilibrium state $\Gamma_0(\alpha)$ where $d\alpha/dt=0$:

$$\Gamma_\alpha\left(\alpha, \frac{d\alpha}{dt}\right) = \Gamma_0(\alpha) + \Gamma_1(\alpha)\frac{d\alpha}{dt} + \Gamma_2(\alpha)\left(\frac{d\alpha}{dt}\right)^2 \geq 0. \tag{9c}$$

Here Γ_1 and Γ_2 are expansion corfficients. In the case of constant damage the deformational process is reversible and entropy production is zero ($\Gamma_\alpha=0$). This condition implies that $\Gamma_0=0$. The entropy production Γ_α should be nonnegative for any level of damage and direction of its evolution including healing (damage decrease) and destruction (damage increase). That is possible only if the second term of the Taylor series, Γ_1, is identically zero and $\Gamma_2>0$. Thus the quadratic term in (9c) is the dominant term of the Taylor series. Back substitution into (9b) gives

$$\Gamma_2\left(\frac{d\alpha}{dt}\right)^2 = -\frac{1}{T}\frac{\partial F}{\partial \alpha}\frac{d\alpha}{dt}. \tag{9d}$$

From (9b) - (9d) the equation of damage evolution has the form

$$\frac{d\alpha}{dt} = -C\frac{\partial F}{\partial \alpha}, \tag{10}$$

where $C=1/\Gamma_2 T$ is a positive function of the state variables describing the temporal rate of the damage process. We note that (10) describes not only damage increase, but also a process of material recovery associated with healing of microcracks, which is favored by high confining pressure, low shear stress, and especially high temperature.

3.2. Elastic Moduli of a Damaged Material

The elastic properties of a damaged solid should depend on the damage level, and quantification of this has been the subject of much research [e.g. *Kachanov*, 1993]. An undamaged solid with $\alpha=0$ is modeled by an ideal linear elastic material governed by Hook's law. At the other extreme, a material with $\alpha=1$ is densely cracked and loses its stability. Below we describe a nonlinear elastic behavior of damaged material for all values of the damage parameter ($0<\alpha<1$), including strain localization and brittle failure.

Many experimental studies measure nonlinear stress-strain relations for rocks and rock-like materials. For example, *Walsh* [1965] showed that Young's modulus of a cracked elastic solid under uniaxial compression is smaller than the modulus of the same solid without cracks; conversely, crack closure under increasing compressive stress causes a gradual increase in the modulus. Opening and closure of microcracks lead to abrupt changes of elastic properties upon stress reversal from tension to compression [e.g., *Weinberger et al.*, 1994]. Various formulations attempt to model such phenomena. The models of Ambartsumyan-Khachatryan [*Ambartsumyan*, 1982] and *Jones* [1977] assume that the compliance (Poisson's ratio divided by Young's modulus) changes when the associated stress component reverses. *Hansen and Schreyer* [1995] consider opening and closing of microcracks to simulate activation and deactivation of damage in terms of continuum mechanics. For materials with a weak nonlinear response, *Lomakin and Rabotnov* [1978] assumed that the elastic moduli depend only on the type of loading. To evaluate the damage effects, *Lyakhovsky et al.* [1997] derive the macroscopic stress-strain relations for a 3-D elastic solid with noninteracting cracks embedded inside a homogeneous matrix, and test the solution against rock-mechanics experiments. The cracks considered are oriented perpendicular either to the maximum tension axis or maximum compression axis. In the first case they dilate during loading, while in the second they contract. The solution for the elastic energy of such a solid was derived following the self-consistent scheme of *Budiansky and O'Connell* [1976]. Following the formulation discussed by *Lyakhovsky et al.* [1997], the elastic potential is written as

$$U = \frac{1}{\rho}\left(\frac{\lambda}{2}I_1^2 + \mu I_2 - \gamma I_1\sqrt{I_2}\right), \tag{11}$$

where λ and μ are Lame constants, $I_1=\varepsilon_{kk}$ and $I_2=\varepsilon_{ij}\varepsilon_{ij}$ are two independent invariants of the strain tensor ε_{ij}, and γ is an additional elastic modulus (summation notation is assumed). The second order term with the new modulus γ accounts for microcrack opening and closure in a damaged material. The term incorporates nonlinear elasticity even for an infinitesimal strain, and it simulates abrupt change in the elastic properties when the loading reverses from compression to tension. Using (8), the stress tensor is derived from (11) as

$$\sigma_{ij} = \left(\lambda - \gamma\frac{\sqrt{I_2}}{I_1}\right)I_1\delta_{ij} + \left(2\mu - \gamma\frac{I_1}{\sqrt{I_2}}\right)\varepsilon_{ij}. \tag{12}$$

The stress-strain relation (12) can be rewritten to mimic the usual form of Hook's law by introducing effective elastic moduli

$$\lambda^e = \lambda - \frac{\gamma}{\xi}; \quad \mu^e = \mu - \frac{1}{2}\gamma\xi, \tag{13}$$

where the strain invariant ratio $\xi=I_1/\sqrt{I_2}$ characterizes the type of deformation as discussed below.

Lyakhovsky and Myasnikov [1987, 1988] discussed the relation between seismic wave velocity and state of stress for the damage rheology model we use. They found that small amplitude harmonic waves propagate in this model as in a linear anisotropic elastic solid with elastic stiffness tensor depending on the initial state of strain. Three different modes of waves exist, one P wave and two S waves. Thus in spite of its initial isotropic formulation and a scalar damage parameter, the present nonlinear elastic model accounts for a stress-induced anisotropy.

The energy in the form of (11) is used below to describe the elastic behavior of a damaged material with intermediate values of the parameter α ($0<\alpha<1$).

Table 1. Matrix $\partial^2 U/\partial\varepsilon_{ij}\partial\varepsilon_{kl}$

	ε_{11}	ε_{22}	ε_{33}	ε_{12}	ε_{13}	ε_{23}
ε_{11}	$\lambda+2\mu-\gamma\xi$ $+\gamma\xi e_1^2-2\gamma e_1$	$\lambda-\gamma(e_1+e_2)$ $+\gamma\xi e_1e_2$	$\lambda-\gamma(e_1+e_3)$ $+\gamma\xi e_1e_3$	0	0	0
ε_{22}	$\lambda-\gamma(e_1+e_2)$ $+\gamma\xi e_1e_2$	$\lambda+2\mu-\gamma\xi$ $+\gamma\xi e_2^2-2\gamma e_2$	$\lambda-\gamma(e_2+e_3)$ $+\gamma\xi e_2e_3$	0	0	0
ε_{33}	$\lambda-\gamma(e_1+e_3)$ $+\gamma\xi e_1e_3$	$\lambda-\gamma(e_2+e_3)$ $+\gamma\xi e_2e_3$	$\lambda+2\mu-\gamma\xi$ $+\gamma\xi e_3^2-2\gamma e_3$	0	0	0
ε_{12}	0	0	0	$2\mu-\gamma\xi$	0	0
ε_{13}	0	0	0	0	$2\mu-\gamma\xi$	0
ε_{23}	0	0	0	0	0	$2\mu-\gamma\xi$

Here $e_i=\varepsilon_i/\sqrt{I_2}$ is a normalized value of the deformation along principal axes "i".

3.3. Loss of Convexity and Strain Localization

Two different mathematical conditions are appropriate for analyzing material stability. The first is convexity of the elastic energy which provides a unique solution of the static problem [*Ekland and Temam*, 1976]. This criterion was adopted and expanded by R. Hill, T.Y. Thomas, J. Mandel, C. Trusdell, and others [*e.g. Bazant and Cedolin*, 1991]. The second is ellipticity of the elasto dynamic equation [e.g., *Rudnicki and Rice*, 1975]. These two conditions are not always identical, especially for nonlinear elasticity [e.g., *Schreyer and Neilsen*, 1996 a, b]. The first condition is a stronger one, and convexity may be lost prior to the ellipticity. For that reason we start with the first condition for material stability.

The maximum possible value of the damage parameter α for a given strain tensor ε_{ij} is defined by the requirement of convexity of the elastic energy U of (11). This condition implies positivity of all eigenvalues of the matrix $\partial^2U/\partial\varepsilon_{ij}\partial\varepsilon_{kl}$ whose dimension is 6x6 for six independent components of the strain tensor (ε_{11}, ε_{22}, ε_{33}, ε_{12}, ε_{13}, ε_{23}). The matrix components in the coordinate system of the principal axes are given in Table 1. The first eigenvalue is equal to

$$x_1=2\mu-\gamma\xi=2\mu^e\geq 0. \tag{14}$$

This condition implies stability against simple-shear deformation. The second and third eigenvalues satisfy the quadratic equation

$$x^2-(4\mu-3\gamma\xi+3\lambda)x+(2\mu-\gamma\xi)^2+$$
$$+(2\mu-\gamma\xi)(3\lambda-\gamma\xi)+(\lambda\gamma\xi-\gamma^2)(3-\xi^2)=0.$$

The roots of this equation are nonnegative if

$$(2\mu-\gamma\xi)^2+(2\mu-\gamma\xi)(3\lambda-\gamma\xi)+$$
$$+(\lambda\gamma\xi-\gamma^2)(3-\xi^2)\geq 0. \tag{15}$$

If either (14) or (15) is not satisfied, the elastic energy is not a convex function of the strain tensor and the static problem has multiple solutions. It can be shown that conditions (14) and (15) coincide with conditions of positivity of the eigenvalues of the acoustic matrices which correspond to two different polarizations of shear waves. Thus loss of convexity of the elastic energy in the present model also provides the criterion for strain localization used by *Rudnicki and Rice* [1975].

3.4. Kinetics of the Damage Process

Equation (10) provides a general form of damage evolution compatible with thermodynamic principles. Practical use of the equation requires an additional functional relation between the damage parameter α and the three elastic moduli λ, μ, and γ. With the current level of experimental constraints, some simple assumptions should be made. Hence we assume linear dependencies of the elastic moduli λ, μ, and γ on damage:

$$\lambda=\lambda_0+\alpha\lambda_r,$$
$$\mu=\mu_0+\alpha\mu_r, \tag{16}$$
$$\gamma=\alpha\gamma_r,$$

where $\lambda=\lambda_0$, $\mu=\mu_0$, and $\gamma=0$ correspond to initial elastic moduli of the uncracked material. Combining equations (10), (11), and (16) yields an equation of damage evolution

$$\frac{d\alpha}{dt}=-C\rho\left(\frac{\lambda_r}{2}I_1^2+\mu_rI_2-\gamma_rI_1\sqrt{I_2}\right), \tag{17}$$

which may be rewritten in the form

$$\frac{d\alpha}{dt}=-C_dI_2\left(\frac{\lambda_r}{2\gamma_r}\xi^2+\frac{\mu_r}{\gamma_r}-\xi\right). \tag{18}$$

The positive coefficient C_d, given by $C\rho\gamma_r$, describes the rate of damage evolution for a given deformation.

To use equation (18) in a 3-D damage evolution model, we employ two additional constraints. The first is that there exists a critical strain invariant ratio ξ_0 which corresponds to a neutral state between healing and degradation of the material. As will be shown in a later section, this is a generalization of friction, which is a widely observed constitutive behavior in rocks and other brittle materials. High shear strain relative to

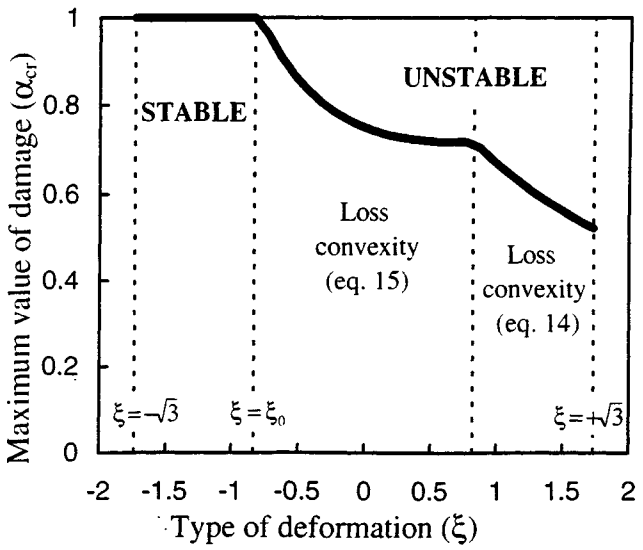

Figure 1. Thick line gives the maximum value (α_{cr}) of the damage parameter α as a function of strain invariant ratio ξ. The range $-\sqrt{3}<\xi<\xi_0$ corresponds to stable behavior with healing. For $\xi>\xi_0$ there is material degradation leading to loss of stability according to equation (14) or (15).

compaction ($0>\xi>\xi_0$) or extension ($\xi>0>\xi_0$) leads to degradation, while high compaction with absence of or low shear component ($\xi<\xi_0$) leads to healing of the material. The coefficient ξ_0 may be estimated from the onset of damage-induced instability or first yielding in rock mechanics experiments. An intuitive possibility for the second constraint, discussed by *Lyakhovsky* [1988] for a similar model, is that of a constant bulk modulus ($\lambda^c+2/3\mu^c$) under isotropic compaction ($\xi=-\sqrt{3}$). However, back substitution to (18) gives with this assumption a zero rate of healing for $\xi=-\sqrt{3}$. This is a significant shortcoming for a model expected to describe earthquake cycles containing both degradation and healing. *Agnon and Lyakhovsky* [1995] slightly changed this assumption and chose only the modulus λ to be constant. Under their condition (16) has the following form

$$\lambda=\lambda_0=\text{const};\quad \mu=\mu_0+\alpha\xi_0\gamma_r;\quad \gamma=\alpha\gamma_r\,, \tag{19}$$

where γ_r is calculated from the conditions (14) and (15) of convexity loss for the maximum value of the damage parameter ($\alpha=1$), when the strain invariant ratio is $\xi=\xi_0$. Figure 1 shows the dependence of the critical damage on the strain invariant ratio for $\lambda_0=\mu_0$. In this case, condition (15) is realized first for $\xi\geq\xi_0$ and prescribes the scale γ_r.

With the assumptions (19), equation (18) is rewritten in a simple form containing only two unknown model parameters

$$\frac{d\alpha}{dt}=C_d I_2(\xi-\xi_0)\,. \tag{20}$$

The two model parameters ξ_0 and C_d are assumed in our model to be material properties. As will be discussed in a subsequent section, the parameters may be constrained by results of rock mechanics experiments. Comparing our model predictions with laboratory data of rate and state-dependent friction, representing average properties of sliding surfaces, we find that in such a context the coefficient C_d does depend on damage. Accordingly, we adopt in that section different rate coefficients (equation 42) for material degradation and healing.

4. General Properties of Damaged Material

In this section, three general properties of the model are analyzed using analytical solutions. The first solution for a 1-D extension problem illustrates strain and damage localization in a previously weakened zone. The second, 2-D case, suggests that there is no stress singularity around a fully destroyed zone. The last example shows that the interaction between the damage evolution and viscous relaxation results in stick-slip shear motion.

4.1. One-Dimensional Deformation

For a uniaxial strain, assuming a linear dependence of Young modulus on damage, $E=E_0[1-\alpha]$, reduces equation (20) to

$$\frac{d\alpha}{dt}=A\left(\frac{\partial u}{\partial x}\right)^2. \tag{21}$$

where u is displacement depending only on the x coordinate, and A is a coefficient which depends on the type of loading. Since in the 1-D case the strain invariant ratio is $\xi=\pm1$, A is one of two constants: $C_d(1-\xi_0)$ for tension or $C_d(-1-\xi_0)$ for compression. Positive and negative values of A correspond to fracturing and healing, respectively. For the 1-D case we consider only a fracturing process.

We investigate the damage evolution of a body with unit length and fixed displacements at the boundaries, $u(0)=0$ and $u(1)=u_0$, in a one-dimensional deformation. These boundary conditions give the body stress

$$\sigma=u_0\left[\int_0^1\frac{dx}{E_0(1-\alpha)}\right]^{-1}, \tag{22}$$

and the strain is given by

$$\frac{\partial u}{\partial x}=u_0\left[E_o\cdot(1-\alpha)\int_0^1\frac{dx}{E_o\cdot(1-\alpha)}\right]^{-1}. \tag{23}$$

Substitution of (23) into (21) results in an equation of damage evolution for the investigated body,

$$\frac{d\alpha}{dt}=Au_0^2\left[\cdot(1-\alpha)\int_0^1\frac{dx}{1-\alpha}\right]^{-2}. \tag{24}$$

For a uniform initial condition ($\alpha|_{t=0}$=const), equation (24) has the solution $\alpha(t)=At$, leading to a complete destruction of the body with finite time. For a nonuniform initial condition ($\alpha|_{t=0}\neq$const), the solution of (24) may be written in the form

$$\alpha(x,t)=1-\frac{1}{E_0}\sqrt[3]{[E_0(1-\alpha(x,0))]^3-f(t)}\,, \tag{25}$$

where f(t) depends on $\alpha(x,0)$. Equation (25) implies that the deformation localizes at a point x_0 which is the maximum of the initial damage distribution. To see that, assume that at some time t' the elastic modulus in the interval $[x_0-c,\ x_0+c]$ may be approximated by a parabola

$$E(x,t')=E_0(1-\alpha(x,t'))=a^2(x-x_0)^2+b^2\,. \tag{26}$$

Substitution of (25) and the parabolic approximation (26) of the modulus into (23) yields a corresponding approximation of the strain distribution in the vicinity of the point x_0.

$$\frac{\partial u}{\partial x} \approx \frac{abu_0}{2\arctan(ac/b)\left[a^2(x-x_0)^2+b^2\right]} \sim \frac{abu_0}{\pi\left[a^2(x-x_0)^2+b^2\right]} \to \delta(x-x_0). \tag{27}$$

Equation (27) shows that the deformation localizes in the vicinity of the point x_0, where the initial damage distribution was maximum, during a process where the damage at x_0 approaches unity or elastic modulus goes to zero ($b/au_0 \to 0$).

Now consider the elastic energy transfer from the relaxing part of the body to surface energy of the localized damaged zone. We assume that $\alpha(x,0)=\alpha_2$ over a small interval of length L, and $\alpha(x,0)=\alpha_1$ ($<\alpha_2$) elsewhere. In this case, the solution of equation (21) may be represented as $\alpha(x,t)=\alpha_2(t)$ at points initially belonging to the interval L, and $\alpha(x,t)=\alpha_1(t)$ elsewhere. On the basis of (24), the two time-dependent functions α_1 and α_2 satisfy

$$\frac{d\alpha_1}{dt} = Au_0^2\left[\frac{1-\alpha_2}{(1-L)(1-\alpha_2)+L(1-\alpha_1)}\right]^2, \qquad \frac{d\alpha_2}{dt} = Au_0^2\left[\frac{1-\alpha_1}{(1-L)(1-\alpha_2)+L(1-\alpha_1)}\right]^2. \tag{28}$$

For small α_1 and α_2 and with $L\to 0$, equations (28) dictate at the initial stage of the damage evolution an increase of α_2 with a rate greater than the rate of increase of α_1. Thus the ratio α_2/α_1 increases with time. This is in line with the previous result on strain localization for a continuous distribution. The damage process localizes in the interval where the initial damage is high. At the final stage of the evolution, with $\alpha_2\to 1$, equations (28) have the solutions

$$\alpha_1 = \text{const}; \qquad \frac{d\alpha_2}{dt} = \frac{Au_0^2}{L^2(1-\alpha_1)^2}.$$

The damage process continues only in the small L interval, where $\alpha(t)$ achieves a unit value at finite time and macroscopic failure of the body occurs. The energy transferred into the high damage region, $G=\int\sigma v dt$, can be written from the previous results as

$$G = L(1-L)u_0^2E_0(1-\alpha_1)^2 \times \int \frac{(1-\alpha_2)\dot{\alpha}_2}{\left[(1-\alpha_1)L+(1-\alpha_2)(1-L)\right]^3}dt. \tag{29}$$

Integrating (29) from a time when $\alpha_2=\bar{\alpha}_2$ to the time of destruction when $\alpha_2=1$, the energy flux G remains finite and is given by

$$G = \frac{E_0u_0^2(1-\alpha_1)}{2(1-L)} - L\frac{E_0u_0^2(1-L)\left[(1-\alpha_1)L+2(1-\bar{\alpha}_2)\right]}{2\left[(1-\alpha_1)L+(1-\bar{\alpha}_2)(1-L)\right]^2}. \tag{30}$$

For the limiting situation $L\to 0$ the energy transfer is $G_0=1/2E_0u_0^2(1-\alpha_1)$. In this case it is seen that all the elastic energy of the relaxed part of the body is transferred to surface energy of the damaged zone. If the rate of the damage process (given by the constant A) is sufficiently large, and/or the length of the initially damaged part is sufficiently small, the rate of the deformational process will increase and part of G_0 will become kinetic and radiate acoustic waves. In this case, only a portion of the initial elastic energy is converted to a surface energy.

4.2. Two-Dimensional Stress Concentration

Extrapolating the results of the previous example to a 2-D case, one may expect strain and damage localization in a small region which leads to stress concentration similar to linear elasticity. However, continuous damage evolution until total destruction eliminates the classical stress singularity. To illustrate that, we analyze stress amplification around a circular hole in a 2-D plate subjected to remote isotropic extension. In a cylindrical coordinate system, only the radial component $\omega_1=\omega(r)$ of the elastic displacements is nonzero, and the stress tensor is given by

$$\sigma_{rr} = \lambda\left(\frac{d\omega}{dr}+\frac{\omega}{r}\right)+2\mu\frac{d\omega}{dr}, \qquad \sigma_{\phi\phi} = \lambda\left(\frac{d\omega}{dr}+\frac{\omega}{r}\right)+2\mu\frac{\omega}{r}, \qquad \sigma_{r\phi}=0. \tag{31}$$

Using (31) in the equation of equilibrium for the linear elastic material gives a general solution in the form

$$\omega(r) = Ar+\frac{B}{r}. \tag{32}$$

From (32) the stress distribution around a circular hole with radius R in the linear elastic plate subjected to remote extension p is

$$\sigma_{rr} = p\left(1-\frac{R^2}{r^2}\right), \qquad \sigma_{\phi\phi} = p\left(1+\frac{R^2}{r^2}\right). \tag{33}$$

The solution has a stress amplification at the boundary ($\sigma_{\phi\phi}|_{r=R} = 2p$) and a $1/r^2$ decay. As a result of this amplification, the damage process starts at the edge of the hole and it is localized in a thin boundary layer having high gradients of damage and elastic moduli variations. The elastic displacement $\omega(r)$ has a corresponding high gradient near r=R, and in that region the term $d\omega/dr$ is dominant in relations (31) for the stress tensor. Neglecting the term ω/r for a finite radius R of the hole, and using the boundary condition $\sigma_{rr}=0$, give instead of (32) the condition $\omega=\text{const}$ ($d\omega/dr=0$) at the boundary. If the damage at the boundary reaches its critical value, the tangential stress component there becomes zero in addition to the radial component. Stress components around the circular hole in a damaged material remain finite even for infinitely small radius of curvature. Instead of singular-like stress distribution, the model predicts an evolving high gradient damage or process zone. The geometry of the process zone and the rate of damage evolution are controlling factors for both the crack trajectory and the rate of crack growth in most engineering materials [*Chudnovsky et al.*, 1990; *Huang et al.*, 1991].

4.3. Stick-Slip Motion

The previous cases neglect viscous stress relaxation and deal only with elastic behavior of damaged material. Here we analyze in one dimension the behavior of a viscoelastic dam-

age material subjected to a constant shear strain rate. For simplicity, the viscosity of the material η is assumed constant. The constitutive relation for a Maxwell viscoelastic body is

$$e = \frac{d}{dt}\left(\frac{\tau}{2\mu}\right) + \frac{\tau}{2\eta}. \quad (34)$$

where τ is shear stress and e is total strain rate (equation 4). As discussed above, the shear modulus μ (equation 19) is assumed to be a linear function of the damage parameter. Thus the equation of damage evolution (20) may be represented by

$$\frac{d\mu}{dt} = C_d \xi_0 \gamma_r \left[\left(\frac{\tau}{2\mu}\right)^2 - \varepsilon_{cr}^2\right]. \quad (35)$$

where ε_{cr} is a critical strain corresponding to the onset of material degradation. For a given dilation I_1, ε_{cr} corresponds to a certain ξ_0. When the deformation is larger than ε_{cr} the damage increases, and when it is lower the damage decreases. Thus the elastic modulus changes together with the damage between zero (loss of convexity and stress drop) and its maximum value. Within these limits the system of equations (34) and (35) has a singular saddle point corresponding to the unstable equilibrium solution

$$\tau = 2\eta e; \quad \mu = \frac{\eta e}{\varepsilon_{cr}}. \quad (36)$$

The two coupled nonlinear equations (34) and (35) describe the temporal variations of shear stress and shear modulus in a damage material subjected to a constant rate of shear strain. The Maxwell relaxation time is $t_v=\eta/\mu$, while a characteristic time scale of the damage process is of the order of $t_d=\mu_0/C_d\gamma_r(\varepsilon^2-\varepsilon^2_{cr})$, or $t_d=\mu_0/C_d\gamma_r\xi_0 I_2(\xi-\xi_0)$ for a 3-D problem. The ratio t_v/t_d controls the style of evolution of the mechanical system. A small t_v/t_d implies that the shear stress τ can increase for a given strain rate without significant change in the elastic modulus of the material. If this stress causes the elastic strain to be less than critical, then stable creep is realized. A higher level of the applied strain rate results in elastic strain larger than the critical, which leads to material degradation and stress drop. No significant material healing is expected after stress drop, and the applied constant strain rate does not produce significant consequent stress.

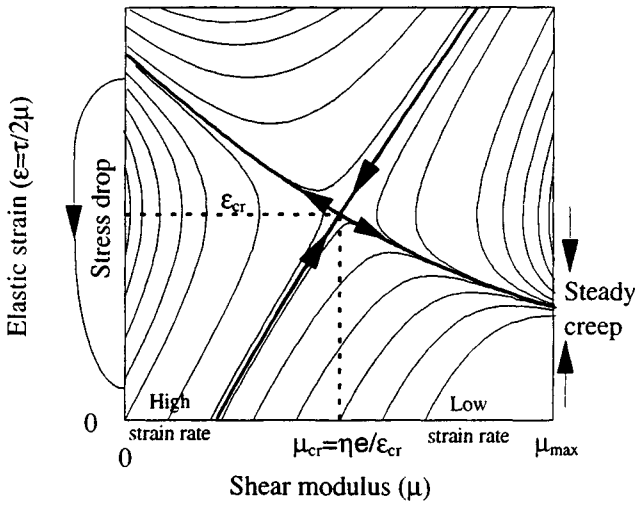

Figure 2. Phase plane with evolution of viscoelastic damage material subjected to a constant strain rate.

The material evolution displays another style if the ratio t_v/t_d is of the order of 1 (Figure 2). Relatively low applied strain rates ($e\sim\mu\varepsilon_{cr}/\eta$) correspond to a set of trajectories tending to stable creep. The shear modulus is increased up to its maximum value and the shear stress approaches the value $\tau=2\eta e$. Higher strain rates ($e>>\mu\varepsilon_{cr}/\eta$) also produce material healing at the initial stage of evolution, but the critical elastic strain ε_{cr} is achieved before the shear modulus obtains the value $\mu_{cr}=\eta e/\varepsilon_{cr}$ (horizontal dashed line in Fig. 2). At this point the damage evolution reverses its direction, and a degradation stage begins, leading to a stress drop. The dynamic stress drop, which is not analyzed here, quickly reduces the elastic strain to some low value, keeping zero shear modulus. There is a locus of trajectories that starts from the line $\mu=0$ and shows significant material recovering together with increase of elastic strain. When the shear stress is large enough, the damage evolution reverses direction again, and a new degradation stage begins, leading to the next stress drop. If the strain rate is so high that the value μ_{cr} is larger than the maximum shear modulus of the material with zero damage, the steady creep can not be realized, and only stick-slip behavior occurs. This process forms a repeating limit cycle which physically corresponds to stick-slip shear motion of the viscoelastic damage material.

5. Estimation of Model Parameters

Savage et al. [1996] draw a connection between macroscopic friction measured on saw-cut specimens and internal friction that characterizes shear fracture of intact rock. They write the strength of an intact rock as the sum over the plane of the incipient fault of both friction on closed microcracks and strength of the remaining grains. The approach taken here extends that connection. We focus our attention on confining pressures sufficient for closure of microcracks, so stress concentration may arise only once the shear stress meets the frictional criterion. Then favorably oriented cracks slide and load their tips giving rise to damage increase (equation 20). The difference between the frictional strength of prefaulted surfaces and the strength of the intact rock is given by the excess stress that is needed to increase the damage from its initial value to critical. That stress difference is rate dependent; since it can be calculated readily from the model, it constrains the rate coefficient C_d. In the limit that the strain remains near-critical for damage growth ($\xi-\xi_0 \to 0$), the time for fracture is infinite, but the strength is friction-like. In this case a smooth surface will evolve along which the damage will approach the critical level ($\alpha\to 1$). These features are explored below analytically, and illustrated by numerical examples. Our main concern here is to estimate the model parameters ξ_0 and C_d which govern the style of damage evolution. The parameter ξ_0 may be estimated from different types of rock mechanics experiments; the parameter C_d is less well constrained.

5.1. Friction and the Onset of Damage

One of the best studied rock property is the friction angle. We relate the critical strain invariant ratio ξ_0 to the friction angle φ by considering the critical shear stress for Mohr-Coulomb sliding:

$$\tau = \tan(\varphi)\sigma_n,$$

where σ_n is normal stress. Consider a saw-cut interface between two intact blocks in a friction experiment carried out

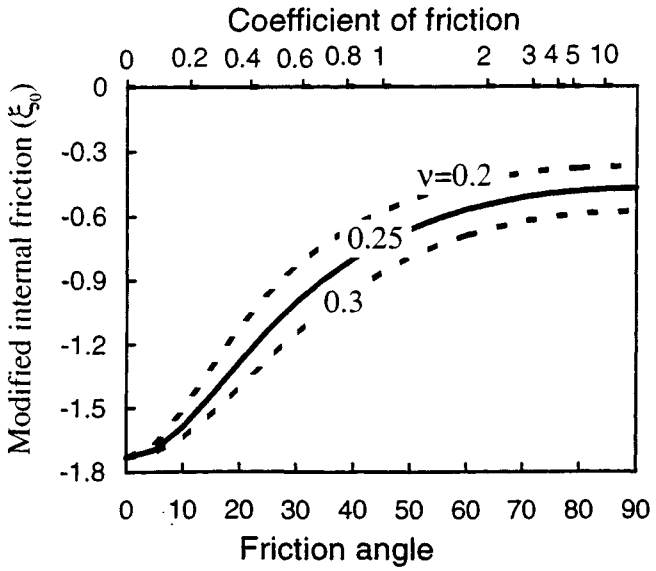

Figure 3. Modified internal friction ξ_0 as a function of friction for different Poisson ratios ν=0.2, 0.25, and 0.3.

under confining pressure. Except for the interface (and perhaps thin adjacent boundary layers), the sample has negligible damage. Stresses are transmitted elastically to the interface, and the corresponding strain can be calculated using Hook's law and conditions of triaxial compression ($\varepsilon_{11}=\varepsilon_{22}>\varepsilon_{33}<0$). The condition for fault slip is then [*Agnon and Lyakhovsky*, 1995]

$$\xi_0 = \frac{-\sqrt{3}}{\sqrt{2q^2(\lambda_e/\mu_e + 2/3)^2 + 1}}, \qquad (37)$$

where

$$q = \frac{\sin(\varphi)}{1-\sin(\varphi)/3}.$$

Physically (37) means that the model parameter ξ_0 is some modification of the internal friction. Figure 3 shows the dependency of the modified internal friction (ξ_0) on the friction for three values of λ_0/μ_0 corresponding to values of Poisson ratio 0.2, 0.25, and 0.3. Thus for Westerly granite with friction angle φ~30° [*Byerlee*, 1967], equation (37) gives ξ_0~−0.8. The result varies little for different rocks with Poisson ratio values between 0.2 and 0.3.

5.2. Three-Dimensional Faulting Experiments

The modified internal friction ξ_0 may also be estimated using results of faulting experiments under 3-D strain fields given by *Reches* [1983]. Figure 4 displays empirical relationships between the first and second stress invariants for the first yielding in those experiments. The data appear to be well approximated by the relation

$$J_2 = rJ_1^2. \qquad (38)$$

Following the notation of *Reches* [1983], the stress invariants are $J_1=\sigma_1+\sigma_2+\sigma_3$, $J_2=\sigma_1\sigma_2+\sigma_1\sigma_3+\sigma_2\sigma_3$. Most of the experimental points for different rock types can be fitted by equation (38) with the empirical coefficient r=0.20-0.27. Assuming that the initial rock samples have negligible levels of damage until the first yielding (i.e., that they behave as linear Hookean solids with elastic moduli λ_0, μ_0) and using Hook's law, the modified internal friction ξ_0 associated with initiation of the damage process is given from the stress (equation 38) as

$$\xi_0 = \frac{-\sqrt{2}}{\sqrt{3(\lambda_0/\mu_0)^2 + 4\lambda_0/\mu_0 + 2 - r(3\lambda_0/\mu_0 + 2)^2}}. \qquad (39)$$

Taking the Poisson's ratio of the rocks close to 0.25 ($\lambda_0\approx\mu_0$), the corresponding range of variation of ξ_0 is found from (39) to be between −0.7 and −1. Our previous estimate based on Byerlee's law for axial symmetric compression experiments (37) falls within this range.

5.3. Onset of Acoustic Emission

The emission of acoustic signals during compressive failure experiments begins at the onset of dilatancy, and this activity accelerates in proportion to the rate of dilatancy which is often observed together with localization of deformation [*Scholz*, 1990 and references therein]. Figure 5a shows observed acoustic emission (AE) data of *Sammonds et al.* [1992], obtained during a deformational experiment on Darley Dale sandstone with a nominal strain rate of 10^{-5} s^{-1} and confining pressure of 50 MPa. After a roughly linear elastic loading in the first 2500 s (axial stress up to 220 MPa) there is a steep rise in AE associated with first yielding and onset of cracking. Material degradation then leads to a second yielding, involving dynamic instability and abrupt stress drop at 3700 s (peak stress of about 290-300 MPa). The observed first and second yielding points can be used to estimate the model parameters ξ_0 and C_d. In our framework, the damage of the sample, initially assumed equal to zero (α=0), starts to increase rapidly at the first yielding when the deformation exceeds the critical value ξ_0. Calculated damage evolution, obtained from equation (20), is similar to the experimental rise in AE rate (Figure 5b). The calculations give loss of convexity, or dynamic stress drop, within a finite period of time and allow us to estimate the second model parameter C_d. We obtain a good fit to the

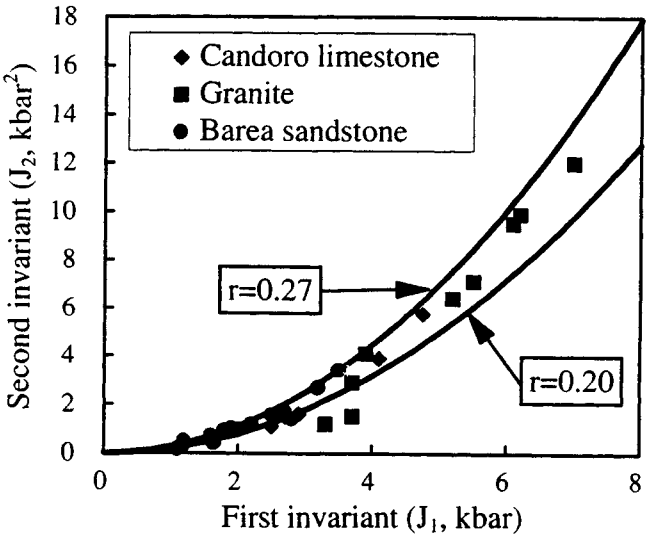

Figure 4. Experimental relations between first ($J_1=\sigma_1+\sigma_2+\sigma_3$) and second ($J_1=\sigma_1\sigma_2+\sigma_1\sigma_3+\sigma_2\sigma_3$) stress invariants at the first yielding under 3-D stress field for different types of rocks [after *Reches*, 1983], and their approximation by equation (38).

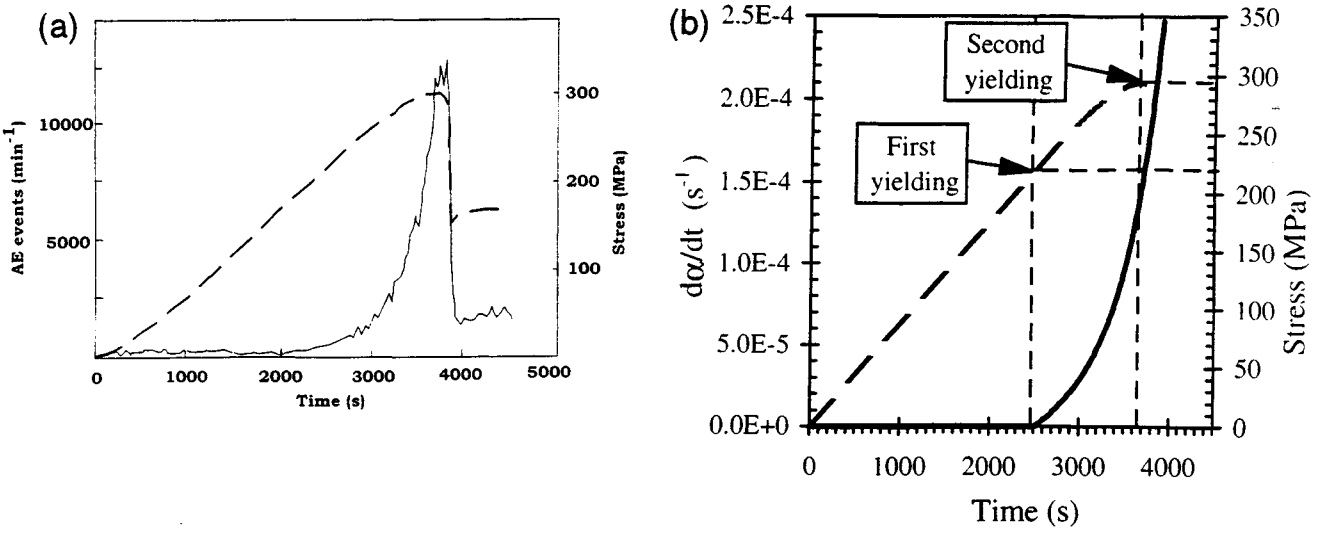

Figure 5. (a) Observed acoustic emission (solid line) and axial stress (dashed line) during deformational experiment on Darley Dale sandstone with a nominal strain rate of 10^{-5} s^{-1} and confining pressure of 50 MPa (Modified with permission from *Nature* [*Sammonds et al.*, 1992]; copyright Macmillan Magazines Limited). (b) Calculated damage evolution ($d\alpha/dt$ - solid line) and axial stress (dashed line) by the damage rheology model with ξ_0=–0.75 and C_d=0.5 s^{-1}.

experimental results of *Sammonds et al.* [1992] with ξ_0=–0.75 and C_d=0.5 s^{-1}. The value of the modified internal friction ξ_0 is again in good agreement with the previous estimates.

5.4. Intact Strength

Most experiments on fracture or intact strength of rocks do not record AE and the first yielding is not defined. Only the second yielding is reported. However, these data also can be used to estimate C_d if the strain rate during the loading is reported and the friction angle is given by the angle of saw-cut samples. Figure 6 shows the results of saw-cut Westerly granite samples after *Stesky et al.* [1974], which are in a good agreement with *Byerlee*'s [1967] friction law for Westerly granite

$$\tau = 0.5 + 0.6\sigma_n \quad \text{(kbar)}.$$

Using the previous estimate (ξ_0=–0.8) for Westerly granite based on the Byerlee friction law, damage evolution is simulated for strain rate of $2.7 \cdot 10^{-5}$ s^{-1} [*Stesky et al.*, 1974] and different values of C_d=1, 3, and 5 s^{-1}. Three lines shown in Figure 6 represent maximum differential stress (stress envelopes) versus confining pressure simulated for the three different C_d. The curve for C_d=3 s^{-1} fits well the experimental data of *Stesky et al.* [1974] and gives another estimate of the damage rate constant.

It appears that the parameter ξ_0 is well constrained and varies little with different types of rocks and loading conditions. The values of the damage rate constant C_d vary by an order of magnitude based on a limited range of experiments with a similar strain rate of about 10^{-5} s^{-1}. Thus additional constraints for C_d with different strain rates are needed. Some of those may come from fitting simulated seismicity patterns of the type discussed in paper 2.

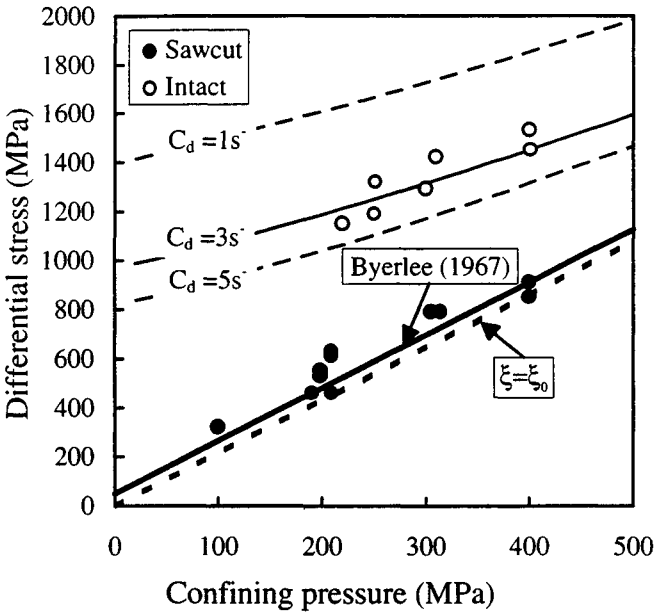

Figure 6. Frictional stress for sawcut series (solid circles) and intact series (open circles) for Westerly granite [after *Stesky et al.*, 1974]. The heavy solid line shows the friction law of *Byerlee* [1967]. The heavy dashed line gives the yielding stress for the modified internal friction ξ_0=–0.8. Thin solid and dashed lines give the simulated yielding stress for C_d=1, 3, 5 s^{-1}.

6. Model Implications

6.1. Necking of Thin Plate

The large-scale extension of thin sheets may, under certain conditions, generate further instabilities by the formation of fault zones or local necks. First we provide an expression for the direction of the neck trace for plastic material. Expressions for a perfectly plastic material were given by *Storen and Rice* [1975] and were used by *Agnon and Eidelman* [1991] for analysis of continental rifts. To maintain a constant length and rigid blocks, the neck must form along horizontal directions of zero extension, or velocity characteristics, symmetrical about

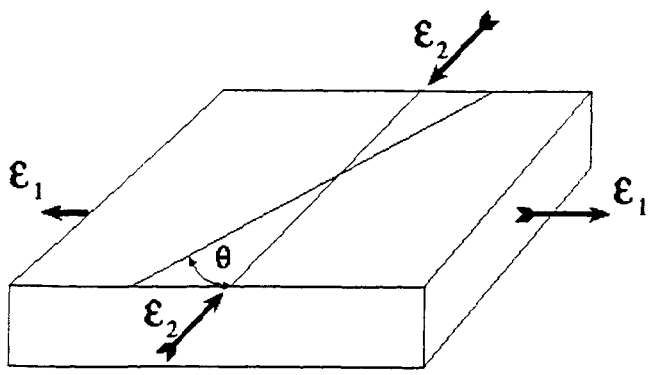

Figure 7. Direction of neck trace in a thin plate with respect to the axis of maximum compression.

the principal incremental strain axes. For incompressible plastic plates, the direction θ between the neck and the axis of maximum compression (Figure 7) is defined by the ratio ρ between the rate of shortening ε_1 and extension ε_2

$$\tan^2(\theta) = \rho = -\frac{\varepsilon_1}{\varepsilon_2}.$$

The orientations of preferred faults in a brittle material were determined by *Reches* [1983] numerically and analytically for different cases. For ρ≤0 the orientation of a fault plane with respect to the coordinate system of the principal strain axes is given from equation (27) of *Reches* [1983]

$$S_1 = \frac{\sqrt{2}}{2}(1+\sin(\varphi))^{1/2},$$

$$S_2 = \frac{\sqrt{2}}{2}|\rho|^{1/2}(1-\sin(\varphi))^{1/2},$$

where S_1 and S_2 are slip directions and φ is a friction angle. The ratio S_1 to S_2 gives the angle θ between the fault plane and axis of maximum compression as

$$\left(\frac{S_1}{S_2}\right)^2 = \tan^2(\theta) = |\rho|\frac{1-\sin(\varphi)}{1+\sin(\varphi)}. \quad (40)$$

Frictional sliding is characterized by ρ=1, and the angle between a fault trace and the axis of maximum compression can be expressed through the Coulomb criterion as θ=±(45°−φ/2). Simple calculations show that equation (40) reproduces exactly this angle for ρ=1.

Figure 8a shows θ for a perfectly plastic plate and a brittle plate with friction angle φ =30°, 40°, 50° (equation 40). Also shown are results of numerical simulations with the present model of damage evolution for a material with the modified internal friction ξ_0=−0.8. This corresponds to a friction angle φ =40° for Poisson ratio ν=0.25 (see Figure 3). Each numerical calculation starts from random initial damage distribution. With time, the damage increases and forms localized zones of very high damage (Figure 8b) with orientation depending on the parameter ρ. The values based on the numerical simulations fit well the prediction of the fault plane orientation in brittle material. These results, and additional simulations discussed in paper 2, illustrate that our damage rheology model is suitable for the study of the evolution of fault branching and other structural irregularities.

6.2. State Dependent Friction and Nonlinear Healing

Following and confirming the pioneering experiments of *Rabinovicz* [1965] on metals, studies of rock friction provide evidence that the static friction increases slowly with the duration of stationary contact [*Dieterich*, 1972]. *Dieterich*

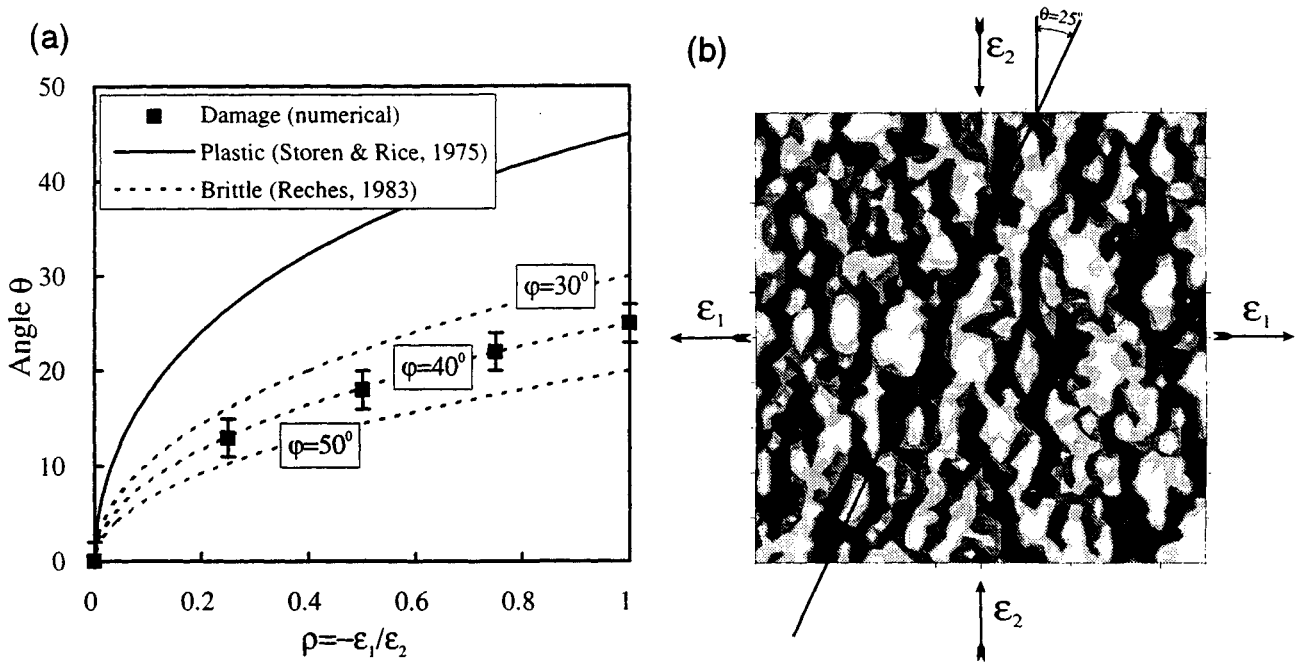

Figure 8. (a) Fault zone orientation in plastic material (heavy line), brittle material with friction angle φ=30°, 40°, and 50° (dashed lines), and model of damage evolution of a material with the modified internal friction ξ_0=−0.8 (squares with vertical bars). The assumed ξ_0 corresponds to the friction angle φ =40° for Poisson ratio ν=0.25 (see Figure 3). (b) Numerical simulation of localized high damage zones in a thin plate under 2-D loading with ρ=−$\varepsilon_1/\varepsilon_2$=1. Bands of connected damage zones have developed at an angle of about 25° to the principal stress direction ε_2.

[1979, 1981]. *Ruina* [1983] and others interpreted results of laboratory friction experiments involving hold times of the pulling mechanism and jumps in sliding velocities in terms of rate- and state-dependent friction. As was mentioned in the introduction, the RS friction, like our model, provides a conceptual framework incorporating all important stages of an earthquake cycle. It is therefore useful to compare results based on our model predictions with laboratory measurements of RS frictional parameters.

In contrast to laboratory frictional experiments, our model does not have sliding surfaces, but rather damaged zones of weakness. Nevertheless, a comparison of our model results with laboratory RS (and other frictional) data is useful, since it allows us to adapt our model to macroscopic situations involving various faulting phenomena.

Following equation (20), material healing starts when the deformation is less than critical ($\xi<\xi_0$). As discussed in the context of Figure 3, for zero initial damage the coefficient ξ_0 may be estimated from the friction of the material. Once this coefficient is fixed, substituting the effective elastic moduli (13) into (37) we may calculate the friction angle as a function of the initial damage (Figure 9). This is not the same as the static friction that is measured in laboratory friction experiments, but both coefficients have a similar physical sense, and they are expected to be proportional to each other [*Savage et al.*, 1996].

Dieterich [1972] reported detailed results of frictional experiments with different normal stress and hold times up to 10^5 s and fitted the static friction with the equation

$$\mu_s = \mu^0 + A \log_{10}(1+Bt), \qquad (41)$$

where t is the duration of the hold time in seconds, $\mu^0 \approx 0.6$-0.8, $A \approx 0.01$-0.02, and $B \approx 1$-2 s^{-1}. The results were interpreted as representing enlargement of the real contact area with time due to indentation creep around geometrical asperities. Using our previous assumption on the relation between α and μ_s and employing equation (20) for material healing under normal stress σ_n, the damage rheology model predicts linear increase of the static friction with time. This relation cannot fit the experimental data, and it leads to a quicker increase of μ_s than the logarithmic law. This suggests that the rate of healing depends on the damage itself. This imposes that for healing the damage rate coefficient is proportional to the exponent of the current level of α. Thus we substitute a function for the parameter C_d in equation (20) to incorporate different coefficients for degradation and healing in the form

$$\frac{d\alpha}{dt} = \begin{cases} C_d I_2(\xi-\xi_0) & \text{for } \xi \ge \xi_0 \\ C_1 \exp(\frac{\alpha}{C_2}) I_2(\xi-\xi_0) & \text{for } \xi \le \xi_0, \end{cases} \qquad (42)$$

where C_d is constant describing the rate of degradation and C_1 and C_2 are constants describing the rate of healing. With this modification the equation for healing has the logarithmic solution

$$\alpha(t) = \alpha_0 - C_2 \ln(10) \times \log_{10}\left(1 - \frac{C_1}{C_2}\exp\left[\frac{\alpha_0}{C_2}\right] I_2(\xi-\xi_0)t\right). \qquad (43)$$

Thus a damage decrease (healing) starts from some initial value α_0 (Figure 10) which is critical value for any type of deformation ξ. Normal compression reduces the actual strain invariant ratio below ξ_0 and provides conditions for healing. According to (43), the healing is logarithmic in time in agreement with *Dieterich* [1972, 1979] and following works. Comparing (43) with equation (41) for static friction, and using the relation between damage and friction (Figure 9), we may suggest that the coefficient $C_2\ln(10)$ should be of the same order as A (i.e., $C_2 \sim 10^{-2}$), and the relation $C_1/C_2 \exp\{[\alpha_0/C_2]I_2\}$ is of the same order as B.

Miao et al. [1995] reported experimental results showing time changes of Young's modulus during the healing of crushed rock salt. In those experiments, Young's modulus increases relatively fast at the beginning of the process. After 2000-3000 min the evolution rate significantly decreases, producing a logarithmic-like relationship between Young's modulus and densification time [*Miao et al.*, 1995, Figure 10]. Our model unifies this observed behavior with the experimental results of Dieterich on state dependent friction.

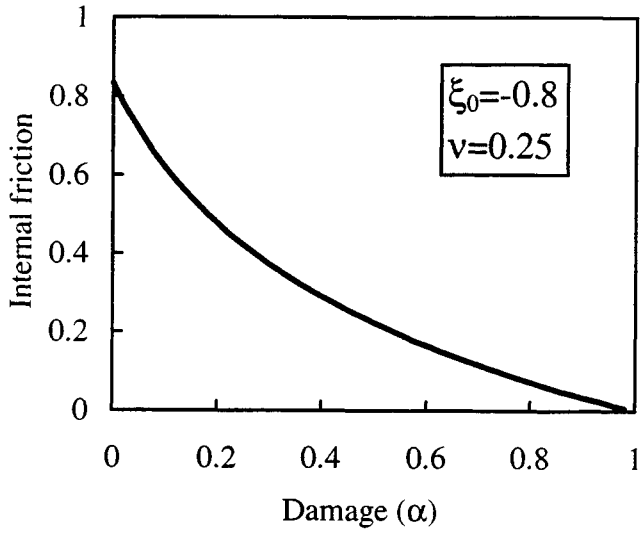

Figure 9. Variation of the friction as a function of damage α.

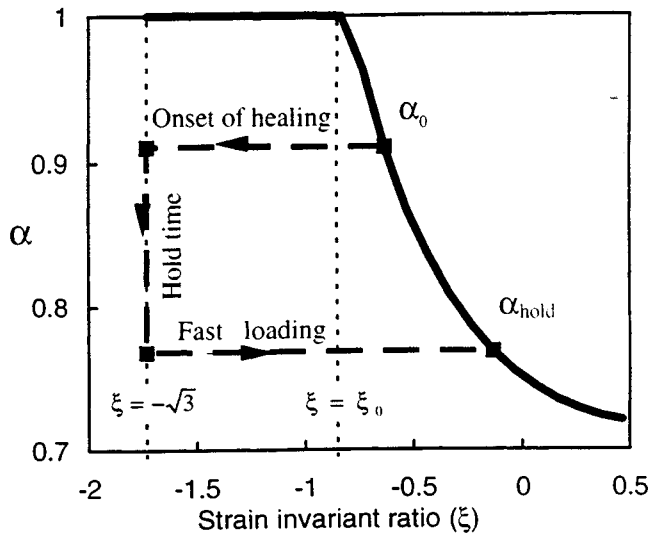

Figure 10. Material recovering in stationary contact from initial damage α_0 to α_{hold} due to normal stress. The increase of static friction is proportional to the logarithm of the hold time duration.

7. Discussion

We have described a damage rheology model based on thermodynamic principles and fundamental observations of rock deformation in situ and in the laboratory. The model has many realistic features of 3-D deformation fields which can be summarized as follows

7.1. Strength Degradation and Healing

A state of stress corresponding to strain $\xi>\xi_0$ leads to material degradation, with a rate proportional to the second strain invariant multiplied by $(\xi-\xi_0)$. Conversly, when $\xi<\xi_0$, the same process results in material strengthening. At each time the existing value of the damage parameter reflects an integrated history of the damage process. The values of the damage rate constants C_d and C_l in equation (42) define the duration of the rock memory for positive (degradation) and negative (healing) damage evolution, respectively. Infinitely large C_d and C_l correspond to zero memory, in which case the model gives ideal elastoplastic behavior. Infinitely small C_d and C_l give Hookean elastic behavior.

7.2. Process Zone

Positive damage evolution starts at low loading when the strain becomes critical ξ_0, and it produces gradual damage in a "process zone" around completely damaged ("destroyed") regions. Because of the finite size of the process zone, our model does not have the unphysical stress singularities of the ideal classical crack solution. The equations of stress have a regular solution at every point, and they incorporate fracture zones having a finite rate of growth. Such process zones are observed in many experiments with rocks and design materials [e.g., *Lockner et al.*, 1991] and their existence often governs the rate and trajectory of the failure evolution.

7.3. Aseismic Deformation, Strain Localization, and Seismic Events

When damage increases, values of the effective elastic moduli decrease, and at some point the elastic energy may lose its convexity. In that situation the slope of the stress-strain relation is negative. The strain localizes in a high damage zone with zero to negative effective moduli, and it may become unbounded if loading continues. The deformation preceding strain localization is stable or with negligible energy loss to seismic emission, while the deformation following strain localization is abrupt or seismic. Thus our model accounts for aseismic deformation, seismic events, and the transitions between these two modes of failure.

Simplified 1-D and 2-D versions of the damage rheology model lead to analytical results incorporating a variety of deformational phenomena, such as strain localization (equation 30) and stick-slip behavior (equation 36). A practical version of the general formulation provides a basic expression (equation 20) for the evolution of damage in terms of two model parameters: a critical deformation ξ_0 separating material degradation from healing, and a constant C_d governing the rate of damage evolution. We have attempted to constrain these parameters with relevant laboratory friction and acoustic emission data (Figures 4-8). Additional constraints are needed, especially for C_d. A variant of the basic damage evolution law, motivated by the time-dependent friction measurements of *Dieterich* [1972], contains two different forms (equation 42) for damage evolution during material degradation and healing. The modified evolution law provides logarithmic healing with time (equation 43) in agreement with the experimental results.

The damage rheology of the present work is used, together with additional developments, in a follow-up paper where we simulate the coupled evolution of regional earthquakes and faults. A number of potential improvements to our damage rheology model should be explored in parallel.

Acknowledgments. We thank J. Lister, Z. Reches, L. Slepyan for useful discussions, and A. Rubin, H. Schreyer, D. McTigue for constructive reviews. A. Agnon acknowledges support from the Binational Science Foundation, grant BSF-92344. V. Lyakhovsky was supported by the Golda Meir Foundation. Y. Ben-Zion was supported by the Southern California Earthquake Center (based on NSF cooperative agreement EAR-8920136 and USGS cooperative agreement 14-08-0001-A0899).

References

Agnon, A., and A. Eidelman, Lithospheric breakup in three dimensions: Necking of a work-hardening plastic plate, *J. Geophys. Res.*, *96*, 20,189-20,194, 1991.

Agnon, A., and V. Lyakhovsky, Damage distribution and localization during dyke intrusion, in The Physics and Chemistry of Dykes, edited by G. Baer and A. Heimann, pp. 65-78, A.A. Balkema, Brookfield, Vt., 1995.

Ambartsumyan, S.A., Raznomodulnaya Teoria Uprugosti (Strain-Dependence Elastic Theory), 320 pp., Nauka, Moscow, 1982.

Anderson, E.M., The Dynamics of Faulting, 183 pp., Oliver and Boyd, Edinburgh, Scotland, 1951.

Andrews, D. J., Rupture propagation with finite stress in antiplane strain, *J. Geophys. Res.*, *81*, 3575-3582, 1976.

Andrews, D. J., Mechanics of fault junctions, *J. Geophys. Res.*, *94*, 9389-9397, 1989.

Andrews, D. J., and Y. Ben-Zion, Wrinkle-like slip pulse on a fault between different materials, *J. Geophys. Res.*, *102*, 553-571, 1997.

Atkinson, B.K., and P.G. Meredith, The theory of subcritical crack growth with applications to minerals and rocks, in Fracture Mechanics of Rock, Academic, San Diego, Calif., edited by B.K. Atkinson, pp. 11-166, 1987.

Aviles, C.A., C.H. Scholz, and J. Boatwright, Fractal analysis applied to characteristic segments of the San Andreas fault, *J. Geophys. Res.*, *92*, 331-344, 1987.

Baer, G., Mechanisms of dike propagation in layered rocks and in massive, porous sedimentary rocks, *J. Geophys. Res.*, *96*, 11,911-11,929, 1991.

Barenblatt, G.I., The mathematical theory of equilibrium cracks in brittle fracture, in Advances in Applied Mechanics, pp. 55-129, Academic, San Diego, Calif., 1962.

Bazant, Z.P., and L. Cedolin, Stability of Structures, Elastic, Inelastic, Fracture and Damage Theories, 984 pp., Oxford Univ. Press, New York, 1991.

Ben-Avraham, Z., and V. Lyakhovsky, Faulting process along the northern Dead Sea transform and the Levant margin, *Geology*, *20*, 1143-1146, 1992.

Ben-Zion, Y., and J.R. Rice, Earthquake failure sequences along a cellular fault zone in a three-dimensional elastic solid containing asperity and nonasperity regions, *J. Geophys. Res.*, *98*, 14,109-14,131, 1993.

Ben-Zion, Y., and J.R. Rice, Slip patterns and earthquake populations along different classes of faults in elastic solids, *J. Geophys. Res.*, *100*, 12,959-12,983, 1995.

Brace, W.F., and D.L. Kohlstedt, Limits on lithospheric stress imposed by laboratory experiments, *J. Geophys. Res.*, *85*, 6248-6252, 1980.

Budiansky, B., and R.J. O'Connell, Elastic moduli of a cracked solid, *Int. J. Solids Struct.*, *12*, 81-97, 1976.

Burridge, R., and L. Knopoff, Model and theoretical seismicity, *Bull. Seismol. Soc. Am.*, *57*, 341-371, 1967.

Byerlee, J.D., Frictional characteristics of granite under high confining pressure, *J. Geophys. Res.*, *72*, 3639-3648, 1967.

Carlson, J. M. and J. S. Langer, Mechanical model of an earthquake, *Phys. Rev. A, 40*, 6470-6484, 1989.

Chai, H., Observation of deformation and damage at the tip of cracks in adhesive bonds loaded in shear and assessment of a criterion for fracture, *Int. J. Fract., 60*, 311-326, 1993.

Chinnery, M.A., Secondary faulting, 1, Theoretical aspects, Can. *J. Earth Sci., 3*, 163-174, 1966.

Chinnery, M.A., Secondary faulting, 2, Geological aspects, *Can. J. Earth Sci., 3*, 175-190, 1966.

Chudnovsky, A., W.-L. Huang and B. Kunin, Effect of damage on fatigue crack propagation in polystyrene, *Polym. Eng. Sci., 30*, 1303-1308, 1990.

Coleman, B.D. and M.E. Gurtin, Thermodynamics with internal state variables, *J. Chem. Phys., 47*, 597-613, 1967.

Cox, S.J.D., and C.H. Scholz, Rupture initiation in shear fracture of rocks: an experimental study, *J. Geophys. Res., 93*, 3307-3320, 1988.

Cowie, P., C. Vanneste, and D. Sornette, Statistical physics model for the spatio-temporal evolution of faults, *J. Geophys. Res., 98*, 21,809-21,821, 1993.

deGroot, S.R., and P. Mazur, *Nonequilibrium Thermodynamics*, 510 pp., North-Holland New York, 1962.

Delaney, P.T., D.D. Pollard, J.I. Ziony, and E.H. McKee, Field relations between dikes and joints: Emplacement processes and paleostress analysis, *J. Geophys. Res., 91*, 4920-4938, 1986.

Dieterich, J.H., Time-dependent friction in rocks, *J. Geophys. Res., 77*, 3690-3697, 1972.

Dieterich, J. H., Modeling of rock friction, 1, Experimental results and constitutive equations, *J. Geophys. Res., 84*, 2161-2168, 1979.

Dieterich, J. H., Constitutive properties of faults with simulated gouge, in *Mechanical Behavior of Crustal Rocks: The Handin Volume, Geophys. Monogr. Ser.*, vol. 24, pp. 103-120, AGU, Washington, D.C., 1981.

Dugdale, D.S., Yielding of steel sheets containing slits, *J. Mech. Phys. Solids, 8*, 100-104, 1960.

Ekland, I., and R. Temam, *Convex Analysis and Variational Problems*, 390 pp., Elsevier, New York, 1976.

Fitts, D.D., *Nonequilibrium Thermodynamics*, 173 pp., McGraw-Hill, New York, 1962.

Freund, L.B., *Dynamic Fracture Mechanics*, 563 pp., Cambridge Univ. Press, New York, 1990.

Gibbs, J.W., *The Scientific Papers*, vol. 1, *Thermodynamics*, New York, 1961.

Hansen, N.R., and H.L. Schreyer, A thermodynamically consistent framework for theories of elastoplasticity coupled with damage, *Int. J. Solids Struct., 31*, 359-389, 1994.

Hansen, N.R., and H.L. Schreyer, Damage deactivation, *J. Appl. Mech., 62*, 450-458, 1995.

Hoek, J.D., Dyke propagation and arrest in Proterozoic tholeitic dyke swarms, Vestfold Hills, East Antarctica, in *The Physics and Chemistry of Dykes*, edited by G. Baer and A. Heimann, pp. 79-95, A.A. Balkema, Brookfield, Vt., 1995.

Hoff, N.J., The necking and rupture of rods subjected to constant tensile loads, *J. Appl. Mech., 20*, 105-108, 1953.

Huang, W.-L., B. Kunin, and A. Chudnovsky, Kinematics of damage zone accompanying curved crack, *Int. J. Fract., 50*, 143-152, 1991.

Hull, J., Thickness-displacement relationships for deformation zones, *J. Struct. Geol., 10*, 431-435, 1988.

Ida, Y., Cohesive force across the tip of longitudinal shear crack and Griffith's specific surface energy, *J. Geophys. Res., 77*, 3796-3805, 1972.

Irwin, G.R., Elasticity and Plasticity, in Handbuch der Physik, vol. VI edited by S. Flugge, pp. 551-590, Springer, Berlin, 1958.

Jones, R.M., Stress-stain relation for materials with different moduli in tension and compression, *AIAA J., 15*, 62-73, 1977.

Ju, J.W., Isotropic and anisotropic damage variables in continuum damage mechanics, *J. Eng. Mech., 116*, 2764-2770, 1990.

Kachanov, L.M., On the time to rupture under creep condition (in Russian), *Izv. Acad. Nauk SSSR, Otd. Tekh. Nauk, 8*, 26-31, 1958.

Kachanov, L.M., *Introduction to Continuum Damage Mechanics*, 135 pp., Martinus Nijhoff, Dordrecht, Netherlands, 1986.

Kachanov, M., Elastic solids with many cracks and related problems, in *Advances in Applied Mechanics*, vol. 30, edited by J. Hutchinson and T. Wu, pp. 259-445, Academic Press, 1993.

Kachanov, M., On the concept of damage in creep and in the brittle-elastic range, *Int. J. Damage Mech., 3*, 329-337, 1994.

King, G., The accommodation of large strains in the upper lithosphere of the Earth and other solids by self-similar fault systems: The geometrical origin of b-value, *Pure Appl. Geophys., 121*, 761-814, 1983.

Lockner, D.A. and J.D. Byerlee, Development of fracture planes during creep in granite, in *2nd Conference on Acoustic Emission/Microseismic Activity in Geological Structures and Materials*, pp. 1-25, Trans Tech., Clausthal-Zellerfeld, Germany, 1980.

Lockner, D.A., and T.R. Madden, A multiple-crack model of brittle fracture, 1, Non-time-dependent simulation, *J. Geophys. Res. 96*, 19,623-19,642, 1991a.

Lockner, D.A., and T.R. Madden, A multiple-crack model of brittle fracture, 1, Non-time-dependent simulation; 2, Time-dependent simulation, *J. Geophys. Res. 96*, 19,643-19,654, 1991b.

Lockner, D.A., J.D. Byerlee, V. Kuksenko, A. Ponomarev, and A. Sidorin, Quasi-static fault growth and shear fracture energy in granite, *Nature, 350*, 39-42, 1991.

Lomakin, E.V., and Yu.N. Rabotnov, Sootnosheniya teorii uprugosti dlya isotropnogo raznomodulnogo tela (Constitutive relationships for the strain-dependent elastic body), *Izv. Akad. Nauk SSSR Mekh. Tverd. Tela, 6*, 29-34, 1978.

Lubliner, J., On the thermodynamic foundations of nonlinear solids mechanics, *Int. J. Nonlinear Mech., 7*, 237-254, 1972.

Lyakhovsky, V., The effective viscosity of a microfractured medium, (in Russian) no. 4, 94-98, 1988. (English translation, *Izv. Acad. Sci. USSR Phys. Solid Earth*, Engl. Transl., *24*(4), 318-320, 1988.)

Lyakhovsky, V.A., Application of the multimodulus model to analysis of stress-strain state of rocks, (in Russian) no 2, 89-94, 1990. (English translation, *Izv. Acad. Sci. USSR Phys. Solid Earth*, Engl. Transl., *26*(2), 177-180, 1990.)

Lyakhovsky, V.A., and V.P. Myasnikov, On the behavior of elastic media with microdisturbances, (in Russian) no 10, 71-75, 1984. (English translation, *Izv. Acad. Sci. USSR Phys. Solid Earth*, Engl. Transl., 20(10), 769-772, 1984.)

Lyakhovsky, V.A., and V.P. Myasnikov, On the behavior of viscoelastic medium with microfractures subjected to extension and shear, (in Russian) no 4, 28-35, 1985. (English translation, *Izv. Acad. Sci. USSR Phys. Solid Earth*, Engl. Transl., 21(4), 265-270, 1985.)

Lyakhovsky, V.A., and V.P. Myasnikov, Relation between seismic wave velocity and state of stress, *Geophys. J. R. Astron. Soc., 2*, 429-437, 1987.

Lyakhovsky, V.A., and V.P. Myasnikov, Acoustics of rheologically nonlinear solids, *Phys. Earth Planet. Inter., 50*, 60-64, 1988.

Lyakhovsky, V., Y. Podladchikov, and A. Poliakov, Rheological model of a fractured solid, *Tectonophysics, 226*, 187-198, 1993.

Lyakhovsky, V., Z. Ben-Avraham, and M. Achmon, The origin of the Dead Sea rift, *Tectonophysics, 240*, 29-43, 1994.

Lyakhovsky, V., Z. Reches, R. Weinberger, and T.E. Scott, Nonlinear elastic behavior of damaged rocks, *Geophys. J. Int., 130*, 157-166, 1997.

Malvern, L.E., *Introduction to the Mechanics of a Continuum Medium*, 713 pp., Prentice-Hall, Englewood Cliffs, N. J., 1969.

Miao, S., M.L. Wang, and H.L. Schreyer, Constitutive models for healing of materials with application to compaction of crushed rock salt, *J. Appl. Mech., 62*, 450-458, 1995.

Mosolov, P.P., and V.P. Myasnikov, Variational methods in flow theory of visco-plastic media, (in Russian), *Prikl. Math. Mekh., 29*, 468-492, 1965.

Myasnikov, V.P., V.A. Lyakhovsky, and Yu.Yu. Podladchikov, Nonlocal model of strain-dependent visco-elastic media, (in Russian), *Dokl. Acad. Sci. USSR, 312*, 302-305, 1990.

Nishihara, M., Stress-strain relation of rocks, *Doshisha Eng. Rev., 8*, 32-54, 1957.

Onsager, L., Reciprocal relations in irreversible processes, *Phys. Rev., 37*, 405-416, 1931.

Okubo, P.G., and K. Aki, Fractal geometry in the San Andreas fault system, *J. Geophys. Res., 92*, 345-355, 1987.

Palmer, A. C., and J. R. Rice, The growth of slip surfaces in the progressive failure of over-consolidated clay, *Proc. R. Soc. London, Ser. A, 332*, 527-548, 1973.

Papa, E., A damage model for concrete subjected to fatigue loading, *Eur. J. Mech. A Solids, 12*, 429-440, 1993.

Papageorgiou, A. S., and K. Aki, A specific barrier model for the quantitative description of inhomogeneous faulting and the prediction of strong ground motion, II, Applications of the model, *Bull. Seismol. Soc. Am., 73*, 953-978, 1983.

Prigogine, I., *Introduction to Thermodynamics of Irreversible Processes*, 115 pp., Thomas, Springfield, Illinois, 1955.

Rabotnov, Y.N., *Creep Problems in Structural Members*, 822 pp., North-Holland, Amsterdam, 1969.

Rabotnov, Y.N., *Mechanics of Deformable Solids*, (in Russian), 712 pp., Science, Moscow, 1988.

Rabinovicz, E., *Friction and Wear of Materials*, pp. 97-99, John Wiley, New York, 1965.

Reches, Z., Faulting of rocks in three-dimensional strain fields, II, Theoretical analysis, *Tectonophysics, 95*, 133-156, 1983.

Reches, Z., Evolution of fault patterns in clay experiments, *Tectonophysics, 145*, 141-156, 1988.

Reches, Z., and D.A. Lockner, Nucleation and growth of faults in brittle rocks, *J. Geophys. Res., 99*, 18,159-18,173, 1994.

Rice, J. R., Spatio-temporal complexity of slip on a fault, *J. Geophys. Res., 98*, 9885- 9907, 1993.

Rubin, A.M., Propagation of magma filled cracks, *Anu. Rev. Earth Planet. Sci. 8*, 287-336, 1995a.

Rubin, A.M., Why geologists should avoid using "fracture toughness" (at least for dikes), in *The Physics and Chemistry of Dykes*, edited by G. Baer and A. Heimann, pp. 53-65, A.A. Balkema, Brookfield, Vt., 1995 b.

Rudnicki, J.W., and J.R. Rice, Conditions for the localization of deformation in pressure-sensitive, dilatant materials, *J. Mech. Phys. Solids, 23*, 371-394, 1975.

Ruina, A., Slip instability and state variable friction laws, *J. Geophys. Res., 88*, 10,359- 10,370, 1983.

Robertson, E.C., Relationship of fault displacement to gouge and breccia thickness, *Min. Eng., 35*, 1426-1432, 1983.

Robinson, E.L., Effect of temperature variation on the long-term rupture strength of steels, *Trans. ASME, 174*, 777-781, 1952.

Sammonds, P.R., P.G. Meredith, and I.G. Main, Role of pore fluids in the generation of seismic precursors to shear fracture, *Nature, 359*, 228-230, 1992.

Savage, J.C., J.D. Byerlee, and D.A. Lockner, Is internal friction friction?, *Geophys. Res. Lett., 23*, 487-490, 1996.

Scholz, C.H., *The Mechanics of Earthquakes and Faulting*, 439 pp., Cambridge Univ. Press, New York, 1990.

Schreyer, H.L., and M.K. Neilsen, Analytical and numerical tests for loss of material stability, *Int. J. Num. Methods Eng., 39*, 1721-1736, 1996a.

Schreyer, H.L., and M.K. Neilsen, Discontinuous bifurcation states for associated smooth plasticity and damage with isotropic elasticity, *Int. J. Solids Struct., 33*, 3239-3256, 1996b.

Sedov, L.I., Variational methods of constructing models of continuos media, in *Irreversible Aspects of Continuum Mechanics*, pp. 17-40 Springer-Verlag, New York, 1968.

Segall, P., and D.D. Pollard, Nucleation and growth of strike slip faults in granite, *J. Geophys. Res., 88*, 555-568, 1983.

Sornette, D., P. Miltenberger, and C. Vanneste, Statistical physics of fault patterns self-organized by repeated earthquakes, *Pure Appl. Geophys., 142*, 491-527, 1994.

Stesky, R.M., W.F. Brace, D.K. Riley, and P.Y.F. Robin, Friction in faulted rock at high temperature and pressure, *Tectonophysics, 23*, 177-203, 1974.

Storen, S., and J.R. Rice, Localized necking in thin sheets, *J. Mech. Phys. Solids, 23*, 421-441, 1975.

Swanson, P.L., Subcritical crack growth and other time and environment-dependent behavior in crustal rocks, *J. Geophys. Res., 89*, 4137-4152, 1984.

Turcotte, D.L., Fractals and fragmentation, *J. Geophys. Res., 91*, 1921-1926, 1986.

Valanis, K.C. A theory of damage in brittle materials, *Eng. Fract. Mech., 36*, 403-416, 1990.

Walsh, J.B., The effect of cracks on the uniaxial elastic compression of rocks, *J. Geophys. Res., 70*, 399-411, 1965.

Ward, S.N., A synthetic seismicity model for Southern California: Cycles, probabilities, and hazard, *J. Geophys. Res., 101*, 22,393-22,418, 1996.

Weinberger, R., Z. Reches, T.S. Scott, and A. Eidelman, Tensile properties of rocks in four-point beam tests under confining pressure, pp. 435-442, in Proceedings First North American Rock Mechanics Symposium, Austin, Tex., 1994.

Weinberger, R., G. Baer, G. Shamir, and A. Agnon, Deformation bands associated with dyke propagation in porous sandstone, Makhtesh Ramon, Israel, in The Physics and Chemistry of Dykes, edited by G. Baer and A. Heimann, pp. 95-115, A.A. Balkema, Brookfield, Vt., 1995.

Yukutake, H., Fracturing process of granite inferred from measurements of spatial and temporal variations in velocity during triaxial deformation, *J. Geophys. Res., 94*, 15,639-15,651, 1989.

A. Agnon and V. Lyakhovsky, Institute of Earth Sciences, The Hebrew University, Givat Ram, Jerusalem, 91904 Israel. (e-mail: vladi@cc.huji.ac.il.)

Y. Ben-Zion, Department of Earth Sciences, University of Southern California, Los Angeles, CA 90089-0740. (e-mail: benzion@terra.usc.edu)

(Received October 29, 1996; revised June 4, 1997; accepted June 30, 1997.)

JOURNAL OF GEOPHYSICAL RESEARCH, VOL. 106, NO. B3, PAGES 4103-4120, MARCH 10, 2001

Earthquake cycle, fault zones, and seismicity patterns in a rheologically layered lithosphere

Vladimir Lyakhovsky
Institute of Earth Sciences, Hebrew University, Jerusalem, Israel

Yehuda Ben-Zion
Department of Earth Sciences, University of Southern California, Los Angeles

Amotz Agnon
Institute of Earth Sciences, Hebrew University, Jerusalem, Israel

Abstract. We study the coupled evolution of earthquakes and faults in a model consisting of a seismogenic upper crust governed by damage rheology over a viscoelastic substrate. The damage rheology has two types of functional coefficients: (1) a "generalized internal friction" separating states associated with material degradation and healing and (2) damage rate coefficients for positive (degradation) and negative (healing) changes. The evolving damage modifies the effective elastic properties of material in the upper crust as a function of the ongoing deformation. This simulates the creation and healing of fault systems in the upper seismogenic zone. In addition to the vertically averaged thin sheet approximation we introduce a Green function for three-dimensional elastic half-space for the instantaneous component of deformation. The formulation accounts in an internally consistent manner for evolving deformation fields, evolving fault structures, aseismic energy release, and spatiotemporal seismicity patterns. These developments allow us to simulate long histories of crustal deformation and to study the simultaneous evolution of regional earthquakes and faults for various model realizations. To focus on basic features of a large strike-slip fault system, we first consider a simplified geometry of the seismogenic crust by prescribing initial conditions consisting of a narrow damage zone in an otherwise damage-free plate. For this configuration, the model generates an earthquake cycle with distinct interseismic, preseismic, coseismic, and postseismic periods. Model evolution during each period is controlled by a subset of physical properties, which may be constrained by geophysical, geodetic, rock mechanics, and seismological data. In the more generic case with a random initial damage distribution, the model generates large crustal faults and subsidiary branches with complex geometries. The simulated statistics depend on the space-time window of the observational domain. The results indicate that long healing timescale, τ_h, describing systems with relatively long memory, leads to the development of geometrically regular fault systems and the characteristic frequency-size earthquake distribution. Conversely, short τ_h (relatively short memory) leads to the development of a network of disordered fault systems and the Gutenberg-Richter earthquake statistics. For intermediate values of τ_h the results exhibit alternating overall switching of response from periods of intense seismic activity and the characteristic earthquake distribution to periods of low seismic activity and Gutenberg-Richter statistics.

1. Introduction

A decade-long surge of activity in the seismological and physics communities is aimed at resolving fundamental questions related to spatiotemporal patterns of earthquakes and faults. These studies typically employ numerical simulations of models based on different conceptual frameworks. Recent summaries and classifications are given by, e.g., *Gabrielov and Newman* [1994] and *Ben-Zion et al.* [1999a]. Most models to date were confined to studies of seismic activity along a single or a few fault systems [e.g., *Robinson and Benites*, 1995]. A few works perform two-dimensional (2-D) calculations of elastostatic deformations in a thin plate to simulate respectively long histories of regional seismicity and the development of regional faults [*Sornette et al.*, 1994; *Ward*, 1996; *Cowie*, 1998, and references therein]. Such 2-D models, however, ignore the coupling of the seismogenic zone to other parts of

Paper number 2000JB900218.
0148-0227/01/2000JB900218$09.00

the lithosphere and fault interactions involving the third dimension. Depth plays a major mechanical role through coupling of the upper seismogenic layer to a viscoelastic substrate. This may produce time-dependent inelastic deformation zones that spread in the ductile lower crust and load faults in the brittle upper layer [e.g., *Lehner et al.*, 1981; *Thatcher*, 1983; *Li and Rice*, 1987; *Ben-Zion et al.*, 1993; *Reches et al.*, 1994]. A second important shortcoming of the foregoing models is that they employ either fixed imposed faults [*Ward*, 1996] or material properties that are constant in time [*Sornette et al.*, 1994], and they thus neglect the fact that the geometry and rheological properties of fault systems evolve with the ongoing deformation [e.g., *King*, 1983; *Andrews*, 1989; *Scholz et al.*, 1993]. *Heimpel and Olson* [1996] simulated lithospheric rifting in models with time-independent properties and approximated Elsasser-type interactions (see section 2) with the depth dimension. Since stress transfer mechanisms in a 3-D rheologically layered solid and the evolution of fault properties with deformation can be important over timescales longer than a few great earthquake cycles, the existing models do not provide conceptually complete frameworks for studying long histories of crustal activity.

In the present work we attempt to overcome the above shortcomings by using a model consisting of an elastic upper layer governed by damage rheology [*Lyakhovsky et al.*, 1997 a, b] over a Maxwell viscoelastic substrate. The calculations employ vertically averaged variables of the thin sheet approximation for the viscous component of motion and a 3-D elastic Green function for the elastic response of the model to deformation. The damage rheology accounts for the creation, evolution, and possible healing of fault zones in the upper crust. The damage approach assumes that the density of cracks is uniform over a length scale much larger than the crack length, yet much smaller than the scale of the macroscopic problem considered. In a specimen under rock mechanics laboratory conditions, microcrack density can be measured over a subcentimeter scale and considered as distributed damage [*Moore and Lockner*, 1995]. On a plate boundary length scale, individual faults that extend to a kilometer length may be considered as distributed damage. The distributed cracks are much smaller than the size of a representative volume, in which crack density is considered homogenous. Hence we define an intensive damage variable α representing the ratio between the elastic shear modulus of a spatial domain relative to the modulus of an ideal crack-free solid. Two aspects of the physics of damage are treated by the present model: (1) a mechanical aspect, the sensitivity of the macroscopic elastic moduli to distributed cracks and to the type of loading, and (2) a kinetic aspect, damage evolution (degradation/recovery of elasticity) in response to ongoing deformation. The theory of the damage rheology and constraints to damage coefficients from laboratory data are discussed in detail by *Lyakhovsky et al.* [1997 a, b] and A. Agnon et al. (manuscript in preparation) and are briefly presented in Appendix A.

In the following, we present theoretical developments relevant to the large-scale structure of the model (layered elastic/viscoelastic half-space). The developed framework allows us to simulate long histories of crustal deformation and to study the simultaneous self-organization of regional earthquake and faults. The model formulation is used to calculate various examples of geodetic fields, evolving upper crust properties, and seismicity patterns and to perform a basic parameter- space study of different dynamic regimes.

2. Model of Crustal Stress Distribution

Strain accumulation and release at a strike-slip plate boundary has been discussed by various authors [e.g., *Sibson*, 1982; *Meisner and Strehlau*, 1982; *Li and Rice*, 1987; *Ben-Zion et al.*, 1993; *Reches et al.*, 1994]. The shallow portion of the lithosphere is generally characterized as elastic and brittle, while the deeper material is assumed to undergo plastic shear flow and creep due to high temperature and pressure. In this work the seismogenic upper crust is governed by damage rheology and is coupled viscoelastically to the substrate, where steady mantle flow drives the deformation. We use different prescribed loads representing various types of mantle flow, ranging from localized step function underneath a single major fault to distributed loading for simulations of regional evolutions of earthquakes and faults.

Most studies of surface deformation around a preexisting plate boundary [*Li and Rice*, 1987; *Ben-Zion et al.*, 1993; *Reches et al.*, 1994] approximate the velocity profile in the mantle with a step-like function. In these models the mantle on either side of the boundary moves with fixed, opposite polarity, velocity parallel to the major fault trace. Such a condition assumes that the mantle flow follows the fault trace, although localization in the asthenosphere is not an anticipated feature. Typical simulations of mantle convection do not lead to strong horizontal shear flow localization even in the colder lithosphere.

Elsasser [1969] developed a vertically averaged thin sheet approximation for a brittle upper crust over a viscous substrate. *Rice* [1980], *Lehner et al.* [1981], and *Li and Rice* [1987] provided a generalized Elsasser model replacing the viscous rheology of the substrate with viscoelasticity. A few attempts have been made to calculate crustal deformation in a 3-D model with a depth-dependent rheology [e.g., *Ben-Zion et al.*, 1993; *Reches et al.*, 1994]. These simulations used the finite element code ABAQUS, and they are very demanding computationally even for modern supercomputers. The results from those studies show that outside the space-time vicinity of a large earthquake, the 3-D calculations do not differ much from those obtained by the Elsasser and

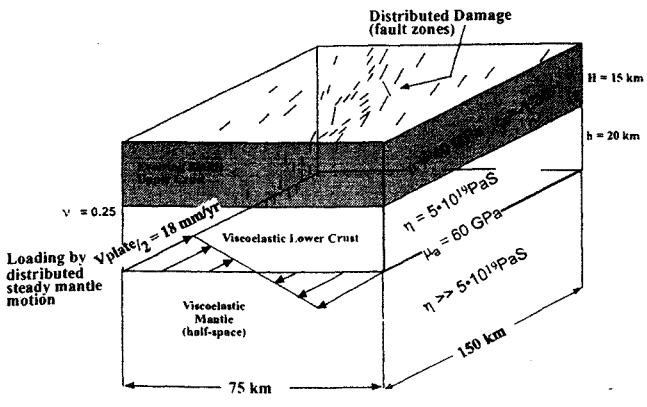

Figure 1. A layered elastic/viscoelastic half-space model. The brittle upper crust (H=15 km) is governed by damage rheology model and is coupled to a viscoelastic lower crust (h=20 km) driven by mantle movement (V_{plate}).

generalized Elsasser models. *Reches et al.* [1994] presented a direct comparison between a thickness-averaged fault-parallel velocity of the elastic layer from 3-D calculations and the analytical solution of *Li and Rice* [1987] for the generalized Elsasser model. After ~50 years into the earthquake cycle the difference between the 2-D and 3-D models is negligible, and at such times both models fit the available geodetic data with about the same accuracy. However, the calculations of *Reches et al.* [1994] and previous results of Rice and coworkers summarized by *Ben-Zion et al.* [1993] show that the generalized Elsasser model is not a satisfactory approximation to deformation in the early part of the earthquake cycle. In section 2.1 we discuss the main features of the generalized Elsasser model and present a hybrid model incorporating 3-D elastic Green function. The hybrid model provides a good approximation of the deformation field even in spatiotemporal domains close to the occurrence of large earthquakes, while being computationally much more efficient than a fully 3-D model.

2.1. Generalized Elsasser Model

Figure 1 shows a model consisting of an elastic upper crust governed by damage rheology over a viscoelastic lower crust with imposed basal loading. For a damage- free upper crust the model corresponds to the framework of *Rice* [1980], *Lehner et al.* [1981], and *Li and Rice* [1987]. The horizontal components of a stress tensor σ_{km} averaged over a thickness H of the upper crust are

$$\sigma_{km}(x,y) = \frac{1}{H}\int_{-H}^{0}\sigma_{km}(x,y,z)dz \qquad (1)$$

Substituting (1) into the 3-D equation of equilibrium gives for the crustal stress distribution,

$$\frac{\partial\sigma_{km}}{\partial x_m} = \frac{\tau_k}{H} \qquad (2)$$

where τ_k is shear traction acting at the boundary between the upper and lower crust layers. This shear traction satisfies an equation of motion of the lower crust, which for a Maxwell viscoelastic element is [*Li and Rice*, 1987]

$$\frac{b}{\mu_a}\frac{\partial\tau_k}{\partial t} + \frac{h}{\eta}\tau_k = \frac{\partial u_k}{\partial t} - V^{(k)}_{plate} \qquad (3)$$

where h, η, and μ_a are thickness, viscosity, and rigidity of the lower crust layer, respectively; $V^{(k)}_{plate}$ is the k-th component of the steady mantle velocity, and b is a scalar discussed below. Expression (3) includes two different terms on the left-hand side. The first describes approximately an instantaneous elastic response of the lower crust to evolving displacement ($\tau_k = \mu_a u_k/b$), and the second corresponds to viscous response of a layer with different velocities on its upper and lower boundaries ($\tau_k = \eta/h\,(\partial u_k/\partial t - V^{(k)}_{plate})$). A term $\rho g H\,\nabla S$, with ∇S giving the slope of the lower-upper crust interface, should be added to the viscous response if the upper crust has a variable thickness. Such cases are not considered here. The coupled equation of stress distribution, obtained by putting (2) into (3), is

$$\frac{Hb}{\mu_a}\frac{\partial}{\partial t}\frac{\partial\sigma_{km}}{\partial x_m} + \frac{Hh}{\eta}\frac{\partial\sigma_{km}}{\partial x_m} = \frac{\partial u_k}{\partial t} - V^{(k)}_{plate} \qquad (4)$$

Lehner et al. [1981] showed that a vertically averaged stress drop in a homogeneous upper crust governed by (4) gives a displacement similar to a mode III crack in an elastic half space if $b \approx (\pi/4)^2 H$. However, this is associated with an exponential decay of the elastic displacements with distance from the fault, while the exact elastic solution follows an algebraic decay. For long-term deformation the elastic field is only a small perturbation around viscous deformation, and the difference between exponential and algebraic decay of the elastic component is not very important. A comparison of deformations generated by an imposed large model earthquake in the generalized Elsasser framework [*Li and Rice*, 1987] and full 3-D simulations [*Reches et al.*, 1994] shows that the former overestimates displacement components have relatively short horizontal wavelengths. However, the difference in thickness-average velocity profile at times larger than tens of years after the earthquake is negligible.

To understand the spatiotemporal evolution of deformation associated with the generalized Elsasser model, we analyze the relaxation time of structures with different length scales by using a Fourier decomposition of a 1-D version of (4). We simplify (4) by assuming that the upper crust obeys Hooke's elasticity and that the deformation field (including imposed plate velocity) has only a "y" component of motion, which depends only on the "x" coordinate (antiplane strain). All material parameters are assumed constant. For these conditions, equation (4) reduces to

$$\frac{Hb\mu}{\mu_a}\frac{\partial}{\partial t}\frac{\partial^2 u}{\partial x^2} + \frac{Hh\mu}{\eta}\frac{\partial^2 u}{\partial x^2} = \frac{\partial u}{\partial t} - V^{(k)}_{plate} \qquad (5)$$

For a zero plate motion ($V_{plate}=0$) we look for a basic solution in the form $u(x,t)=f(t)\,\varphi(x)$. With this equation (5) becomes

$$\frac{Hb\mu}{\mu_a}\dot{f}\varphi'' + \frac{Hh\mu}{\eta}f\varphi'' = \dot{f}\varphi \qquad (6)$$

which may be separated into two equations:

$$\frac{\frac{Hb\mu}{\mu_a}\dot{f} + \frac{Hh\mu}{\eta}f}{\dot{f}} = \frac{\varphi}{\varphi''} = -\lambda^2 \qquad (7)$$

This procedure gives a basic solution to (5) in the form

$$\varphi = A\cdot exp\left(i\frac{x}{\lambda}\right)$$

$$f = B\cdot exp\left(-\frac{hH\mu/\eta}{\lambda^2 + bH\mu/\mu_a}t\right) \qquad (8)$$

According to this solution, the relaxation time of spatial structure with a horizontal wavelength λ is

$$t^* = \frac{\lambda^2 + bH\mu/\mu_a}{hH\mu/\eta} \qquad (9)$$

In the short wavelength limit ($\lambda\to 0$) the relaxation time approaches $b\eta/h\mu_a$. For long wavelenghts ($\lambda\to\infty$) we obtain $t^*=\lambda^2\eta/hH\mu$, which also represents the relaxation time for the original Elsasser model corresponding to $b=0$. Figure 2 shows how the relaxation time changes as a function of wavelength between these limits. Figure 2 also shows the relaxation time for a new hybrid model described in section 2.2 and used later in our work.

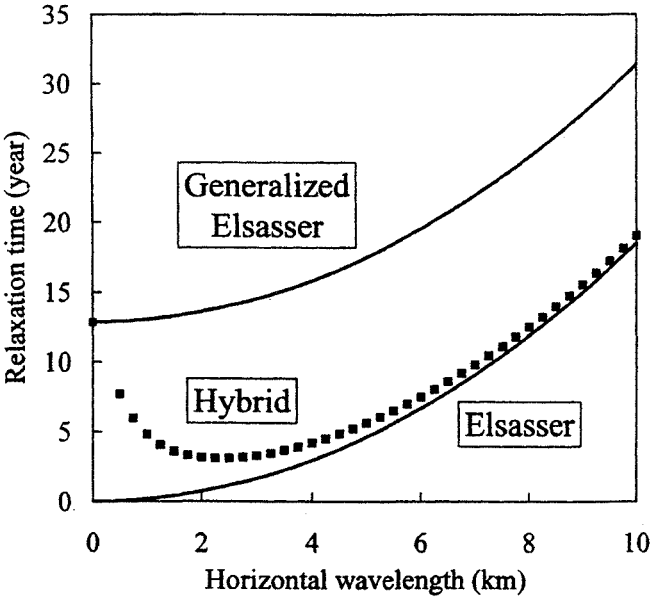

Figure 2. Relaxation time versus horizontal wavelength for the Elsasser and generalized Elsasser models (heavy lines). The numerically calculated relaxation time for the hybrid model (symbols) is similar to that of the generalized Elsasser model for very short length scales, but it approaches the Elsasser solution for long wavelengths (viscosity of the lower crust η=5 10^{19} Pa s).

2.2. A Hybrid Model Incorporating 3-D Green Function

As mentioned above, the substitution $\tau_k=\mu_a u_k/b$ essential to the generalized Elsasser model does not reproduce correctly the elastic component of deformation of the lower crust. Our proposed modification of that model follows the usual seismological assumption [e.g., *Kasahara*, 1981; *Stein et al.*, 1994] that the instantaneous response of the Earth to a sudden stress redistribution is accommodated by an elastic half-space. This assumption is realistic, since the relaxation of strain is not instantaneous even with a lower crust of extremely low viscosity. For example, with a viscosity of 10^{19} Pa s the Maxwell relaxation time is of the order of tens years.

We represent the horizontal displacement field at the boundary between the upper and lower crust layers as a sum of two components: elastic ($u_k^{(e)}$) due to instantaneous deformation in the upper crust and viscous ($u_k^{(v)}$) due to slow flow in the lower crust:

$$u_k = u_k^{(v)} + u_k^{(e)} \tag{10}$$

Equating the stress on the both sides of the lower-upper crust interface, the rate of viscous flow is

$$\frac{\partial u_k^{(v)}}{\partial t} = \frac{h}{\eta}\tau_k + V_{plate}^k \tag{11}$$

For the elastic part of the displacement field we use a 3-D Green function (G_{kn}) in an elastic half-space. The elastic displacement at the boundary surface (S) between the lower and upper crust layers is claculated as a convolution of G_{kn} with forces acting at S:

$$u_n^{(e)} = \iint_S G_{kn}\tau_k\, ds \tag{12}$$

Taking partial derivative of (12) with respect to time, combining the result with (10) and (11), and substituting back into (2) gives the equation of motion for the hybrid model:

$$H\iint_S G_{kn}\frac{\partial}{\partial t}\frac{\partial \sigma_{nm}}{\partial x_m}ds + \frac{hH}{\eta}\frac{\partial \sigma_{nm}}{\partial x_m} = \frac{\partial u_k}{\partial t} - V_{plate}^{(k)} \tag{13}$$

A strictly rigorous Green function for our calculations would account for the varying topography and varying elastic properties simulated by our model (see section 3) and for the fact that the forces operate at a depth H (=15 km here) below the free surface. However, since elsewhere we use in the model the thin sheet approximation (i.e., vertically averaged variables), we employ a Green function for a homogeneous elastic half space [*Landau and Lifshitz*, 1970] multiplied by the thickness of the upper layer, instead of precise integration along vertical direction inside the upper crust. The Green function components become

$$G_{xx} = \frac{H}{2\pi\mu_a}\left(\frac{1-\nu}{r} + \frac{\nu x^2}{r^3}\right)$$

$$G_{yy} = \frac{H}{2\pi\mu_a}\left(\frac{1-\nu}{r} + \frac{\nu y^2}{r^3}\right) \tag{14}$$

$$G_{xy} = \frac{H}{2\pi\mu_a}\frac{\nu xy}{r^3}$$

where r is a radius vector from the origin ($r^2=x^2+y^2$) and ν is the Poisson ratio.

Equation (13) differs from (4) of the generalized Elsasser model by incorporating a 3-D elastic response to rapid stress variations. Below we refer to the framework described by (13) as a "hybrid model". Similar to the analysis in the context of (4-9), we may calculate the relaxation time of spatial structures in the hybrid model with horizontal wavelength λ from (13) as

$$t^* = \frac{\lambda^2 + H\mu\tilde{G}_{xx}(\lambda)}{hH\mu/\eta}$$

where $\tilde{G}_{xx}(\lambda)$ is the Fourier transformation of the Green function. The solid squares in Figure 2 show the calculated relaxation time for different wavelengths in the hybrid model incorporating the Green function (equation (14)). The relaxation time of this model is similar to that of the generalized Elsasser model for very short length scales, but it approaches the basic Elsasser solution for long wavelengths. The spectral response of the hybrid model, bridging the Elsasser and generalized Elsasser models, corrects the shortcoming of the latter framework associated with overestimation of the lifetime of localized stress anomalies after brittle failures. This shortcoming leads to significant local deviations from 3-D calculations [e.g., *Ben-Zion et al.*, 1993; *Reches et al.*, 1994] during the first few years after rapid slip events. This is illustrated in Figure 3 where we compare fault parallel velocity at two normal distances from the fault as a function of time, calculated with the generalized Elsasser model [*Li and Rice*, 1987, equation A6] and our hybrid model.

3. Upper Crust Deformation and Damage Evolution

Our model of a lithosphere, incorporating upper crust material governed by damage rheology over a viscoelastic

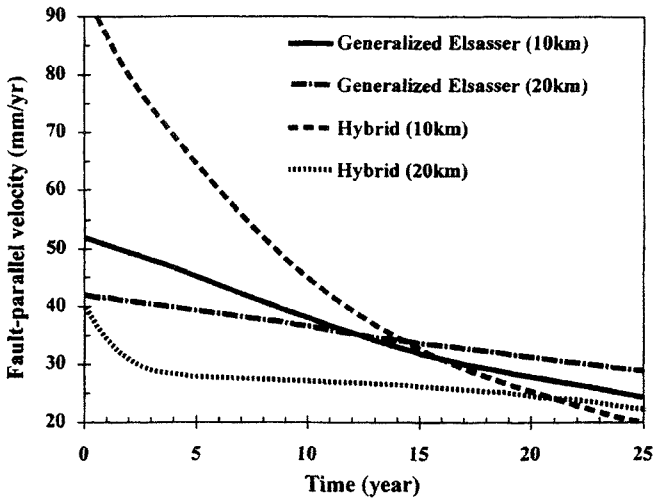

Figure 3. Fault-parallel velocity at two normal distances 10 and 20 km from the fault as a function of time after a seismic event, calculated with the generalized Elsasser model [*Li and Rice*, 1987, equation (A6)] and simulated with the hybrid model.

substrate, can simulate four stages of a seismic cycle: preseismic, coseismic, postseismic, and interseismic deformations. These stages may be anticipated from the behavior of a viscoelastic damaged material: a stick-slip behavior appears if the viscous relaxation time of the nondamaged medium τ_r is longer than the loading time scale τ_l (inverse strain rate) [*Lyakhovsky et al.*, 1997a]. The slip instability corresponds to the coseismic stage. The interseismic stage, spanning most of the stick period between the postseismic and preseismic stages, is represented by a fast healing and localization of damage, respectively (A. Agnon et al., manuscript in preparation).

The hybrid version of the lithospheric model (Figure 1) generates an earthquake cycle under constant loading. Each element of a two-dimensional horizontal mesh may follow a stick-slip cycle, and the collective behavior of a group of elements model the faulting process and macroscopic earthquake failure. When deformation in an element reaches a threshold state, damage starts to increase with degradation of elastic moduli and concentration of elastic strain. This spatially localized initial perturbation in strain corresponds to the preseismic stage, with small geodetic signals at the free surface (possibly below the typical detection limit). A critical damage level for brittle instability marks the onset of the coseismic stage during which the local stress drops. This local stress drop may provide a nucleus for rupture that propagates by reloading the other elements to the critical level. The rupture propagation process continues as long as one or more elements experience brittle failure. When no element sustains brittle instability, the model earthquake ends. The brittle failure leads to an increase in the cumulative irreversible plastic strain, corresponding to the coseismic slip in models that idealize the fault zone as a surface.

The instability during a stress drop requires that we specify the subsequent stress conditions. Earthquake slip histories inferred from observed seismograms [*Heaton*, 1990], laboratory experiments [e.g., *Brune et al.*, 1993; *Anooshehpoor and Brune*, 1999], theoretical models [e.g., *Mora and Place*, 1994; *Andrews and Ben-Zion*, 1997], and a variety of geophysical observations summarized by *Ben-Zion and Andrews* [1998] suggest that earthquake ruptures propagate in the form of narrow slip pulses associated with strong local dynamic stress drops. A complete local stress drop is a physical consequence of the damage mechanics approach since the instability is associated with a vanishing elastic modulus [*Lyakhovsky et al.*, 1997a]. Averaged stress drop along a sliding narrow damage zone reproduces rate- and state-dependent friction (A. Agnon et al., manuscript in preparation). Thus, following a model earthquake, the deviatoric stress is fully dropped locally and the crustal stress is rendered lithostatic, favorable for healing of damage in the postseismic stage. This stage may last from a fraction of a year to a few years, depending on the rate of material recovery.

The imposed plate velocity distribution, the length scales for the lithospheric layers, and the rheological coefficients of each layer comprise the parameters of the model. Some of the parameters can be constrained directly from geophysical data. The structural and kinematic values chosen follow a simplified Californian crust with a representative thickness of 35 km [*Fuis and Mooney*, 1990] sheared between plates moving at the surface with differential velocity of 36 mm/yr. Seismic activity is mostly restricted to the upper 10-15 km. We therefore use H=15 km and h=20 km in the simulation (Figure 1). From seismic refraction and other data [*Fuis and Mooney*, 1990; *Mooney et al.*, 1998] the average rigidity of the crust is estimated at 35-40 GPa for the upper crust and 40-70 GPa for the lower crust and upper mantle. Since the elastic moduli weaken with damage, a reference upper bound of μ=40 GPa is chosen for damage-free upper crust rigidity. Below we constrain simulation results with geodetic data to obtain lower crust viscosity (η) and rigidity (μ_a). We also provide additional details on each stage of deformation evolution and discuss the role of the remaining parameters. We begin the survey of the parameter space with a simplified model that contains a single straight preexisting fault zone.

3.1. A Single Fault System

To study the model setting in incremental complexity level, we start with a step-like profile of the mantle velocity driving the fault. This profile leads to strain localization and damage evolution in a narrow zone above the step that is set in the center of the model (x=0), while other regions in the crustal model develop no damage. With an appropriate choice of boundary conditions the numerical simulation is required only in a small portion of the space around the fault zone. The interaction of the model region with the outer part of the lithosphere is represented by the boundary conditions at the horizontal edges of the model. Periodic boundary conditions at the edges normal to the fault trace represent infinite repetitions of the fault segment along strike. Conditions at the edges parallel to the fault zone should mimic steady plate motion away from the fault zone. *Andrews* [1978] and *Wdowinski and O'Connel* [1990] give useful discussions of the interaction between fault slip and the chosen boundary conditions. The condition ($V=V_{plate}$ for $x\rightarrow\infty$) may be replaced for a finite model as either (1) constant and uniform fault-parallel velocity ($V=V_{plate}$ for $x=\pm L$) or (2) constant and uniform shear stress (σ_{xy}=const for $x=\pm L$). These seemingly equivalent boundary conditions generate very different solutions for fault-parallel velocity and stress distributions during the interseismic period. To illustrate the different behavior under the two types of boundary conditions, we

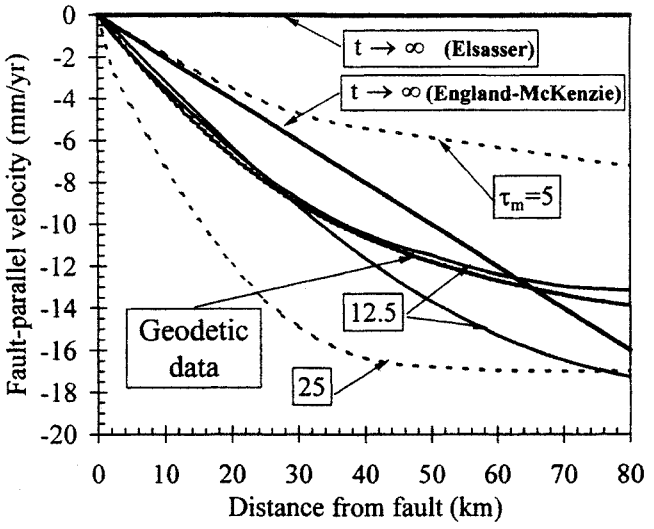

Figure 4. Velocity profiles 100 years after a large earthquake simulated for model relaxation times τ_m=5, 12.5, and 25 years. The shaded line represents the best fit of geodetic data with dislocation model after *Savage* [1990]. Two asymptotic solutions (time→∞) for Elsasser and England-McKenzie boundary conditions are also shown.

examine the quasi-static limit appropriate for the long-term ($t\to\infty$) asymptotic solution by neglecting the temporal derivative on the left-hand side of (13). In the case of constant velocity boundary condition the velocity profile in the model is a straight line ($V(x)=V_{plate}\ x/L$) between zero velocity at the locked fault zone (V=0, x=0) and plate velocity at the boundary ($V=V_{plate}$, $x=\pm L$). This leads to unbounded increase of stress in the upper crust independently of the viscosity of the lower crust and the rate of motion in the upper mantle. *England and McKenzie* [1982], who used a thin sheet viscous model for the problem of long-term continental deformation assumed a similar decoupling between the plate and the substrate. This "England-McKenzie loading" does not provide an appropriate description for relatively short-term brittle-elastic behavior of the upper crust. By contrast, the constant stress boundary condition leads to zero velocity profile and uniform stresses equal the sum of the stress applied at the boundary and the loading from the mantle. In this case the stress in the model region depends on the viscocity of the lower crust and the rate of motion at the bottom of the model. This "Elsasser loading" [*Elsasser*, 1969] corresponds to a situation where the mantle-crust interaction is an essential part of the crustal processes. Since our simulations include short-term processes of brittle failure in the upper crust, we use the Elsasser loading.

During the interseismic period the damage is approximately frozen, and damage evolution does not significantly affect the strain rate of the upper crust. Thus the velocity profile in this period is governed mainly by two model parameters: the imposed mantle velocity and the viscosity of the lower crust. In the following, the mantle velocity is chosen to give far field surface velocity of 1/2 V_{plate}= 18 mm/yr, hence long-term slip velocity is 36 mm/yr. Figure 4 shows simulated surface velocity profiles during the interseismic stage, 100 years after the last seismic event, for various relaxation times (τ_m) defined as

$$\tau_m = \frac{\pi^2}{16}\frac{H}{h}\frac{\eta}{\mu_a}$$

The definition of τ_m is based on the solution of the generalized Elsasser model for the elastic layer (equation (9) with λ=0). The relaxation times used in Figure 4 are τ_m=5, 12.5, and 25 years. The lower value corresponds to $\eta=2.5\times10^{19}$ Pa s and μ_a=60 GPa. The intermediate one corresponds to $\eta=5\times10^{19}$ Pa s and μ_a= 60 GPa, or $\eta=3\times10^{19}$ Pa s and μ_a=40 GPa. The value τ_m=25 years corresponds to $\eta=10^{20}$ Pa s and μ_a=60 GPa.

Observed interseismic fault parallel velocities in geodetic measurements are particularly easy to model in the case where the fault is long and straight and the deformation is uniform in the direction of fault strike. In that case a screw dislocation in an elastic half-space is sufficient to model the observed velocity field at the free surface [*Savage*, 1980] as

$$V = V_0\frac{1}{\pi}\arctan\left(\frac{x}{D}\right)$$

This profile, shown in Figure 4 with a shaded line for slip velocity V_0=36 mm/yr and dislocation depth D=30 km, provides the best fit [*Savage*, 1990] to interseismic geodetic data for the San Andreas Fault in the Transverse Ranges of southern California. *Lisowski et al.* [1991] show that a model with one dislocation fits the geodetic data even better than a multidislocation model. They also show that this fit corresponds to the middle part of the earthquake cycle time T (0.4-0.6 T) by comparison with the compiled data of *Thatcher* [1983].

Our model does not produce an exact arctangent velocity profile. On the basis of the solution of *Chinnery* [1961] the fault parallel elastic component of the displacement (12) with the Green function (14) generated by a stress drop localized along a straight fault follows an arctangent profile [*Kasahara*, 1981, equation 4.30]. The deformation field in our model has additional nonelastic components. Nevertheless, the calculated velocity profiles in Figure 4 at 100 years after the earthquake (the middle part of simulated 200-year earthquake cycle) are very similar to arctangent curves. As shown in Figure 1, we consider a model with H=15 km, h=20 km, and a horizontal extent of 150 km × 75 km. The shear modulus and the Poisson ratio of the damage-free upper crust material are μ=40 GPa and ν=0.25, respectively, and the Poisson ratio of the lower crust is ν=0.25. We try two different values of the lower crust shear modulus μ_a=40 and 60 GPa, and three different values of the lower crust viscosity $\eta=10^{20}$, $5\ 10^{19}$, and $2.5\ 10^{19}$ Pa s. The line with τ_m = 12.5 years ($\eta = 5\ 10^{19}$ Pa s, and μ_a = 60 GPa) fits well the geodetic arctangent model. We use these parameters for all simulations to follow.

The interseismic period lasts until the current strain diagonality ξ (see Appendix A) is below a critical value ξ_0 separating states of damage increase (degradation) and decrease (healing) [*Lyakhovsky* et al., 1997a]. This coefficient was estimated to vary between −0.8 and −1.0 using laboratory data on damage onset, Coulomb friction, and internal friction. In the current simulation, ξ_0 together with a prescribed width of the damage zone control the duration of the interseismic period and therefore the length of the earthquake cycle for a model with a single fault. In this work we use triangular elements of 2.5 km x 2.5 km. This gives a lower bound to the fault zone width in the simulations. Computational limitations prevent us from using a smaller

grid size that maybe more appropriate for natural fault zones. A smaller grid size would define the lower magnitude cutoff for the simulated earthquakes, mildly affect our choice of ξ_0, but not the main conclusions of this work. The grid size dependency of some results is discussed further below.

Exploratory simulations indicate that for the prescribed 36 mm/yr rate of plate motion and average (effective) lithostatic (confining) pressure $p=(\rho-\rho_w)gH/2=0.1$ GPa (using $\rho=2500$ kg/m^3 and $\rho_w=1000$ kg/m^3), the shear strain in the upper crust never reaches values of ξ_0 inferred from the laboratory data for typical intact crustal rocks. Figure 5 shows that the change of current strain diagonality ξ with time during the inter-seismic period is very small. After ~100 years, ξ is almost constant, and thus a small variation in the material property ξ_0 has strong effects. With the increase of ξ_0 from −1.40 to −1.35 the length of the cycle increases by more than twice, from ~80 years to ~190. Further increase of ξ_0 gives even a stronger incremental effect. As shown in Figure 3 of *Lyakhovsky et al.* [1997a], ξ_0 =−1.35 corresponds to an internal friction of ~0.3 for the Poisson ratio equal to 0.25. It is reasonable to expect that the value of internal friction characterizing a wide insitu gouge zone with internal cracks (i.e., damage) is smaller than laboratory values associated with small rock samples. A low value of friction coefficient is compatible with the lack of localized frictional heat along the San Andreas Fault [e.g., *Brune et al.*, 1969, *Lachenbruch and Sass*, 1973], calculations of changes in seismicity rates [*Simpson and Reasenberg*, 1994] and analysis of aftershock mechanisms [*Zoback and Beroza*, 1993] following the Loma Prieta earthquake, simulated b-values on faults in elastic half-space [*Robinson and Benites*, 1995], and calculations of stress transfer favoring observed earthquake histories [e.g., *Harris and Simpson*, 1996; *Stein et al.*, 1997].

The damage model of brittle material does not include any prescribed surfaces that represent planar faults. Instead, we have fault zones associated with regions of high damage having a minimum width equal to the size of one numerical element. While a finite fault zone width is more realistic than a fault surface idealization, the existence of a prescribed minimum fault zone width makes some simulation results, like details of the evolving fault zone geometry and minimum model earthquake, dependent on the numerical cell size. This also renders our model inherently discrete in the sense of *Rice* [1993] and *Ben-Zion and Rice* [1995]. The smallest simulated earthquake whose source occupies one element has a vertical size equal to the thickness of the upper crust and should have a magnitude $M\geq 6$. For given loading and material parameters of the model, this lower cutoff defines an appropriate element size. The isometric cell choice for the simulation, instead of a narrow and elongated one, eliminates any preferred direction related to the numerical procedure. The amount of energy released during a seismic event is proportional to stress drop multiplied by the volume of the elements involved in the rupture process. This energy scales linearly with the width of the damage zone. Similarly, the seismic moment of a simulated earthquake and the associated plastic strain (see below) also increase proportionally to the width. The rate of elastic energy accumulation does not depend on the element size, but the energy release rate is proportional to it. Thus the change of element size leads to proportional change of the duration of the earthquake cycle for a model with a single fault. However, this effect is much weaker than that induced by small changes of the critical strain diagonality (see Appendix A), and it may be compensated by a small variation of ξ_0. The focus of this work is on different possible dynamic regimes of evolving seismicity patterns for a major strike-slip

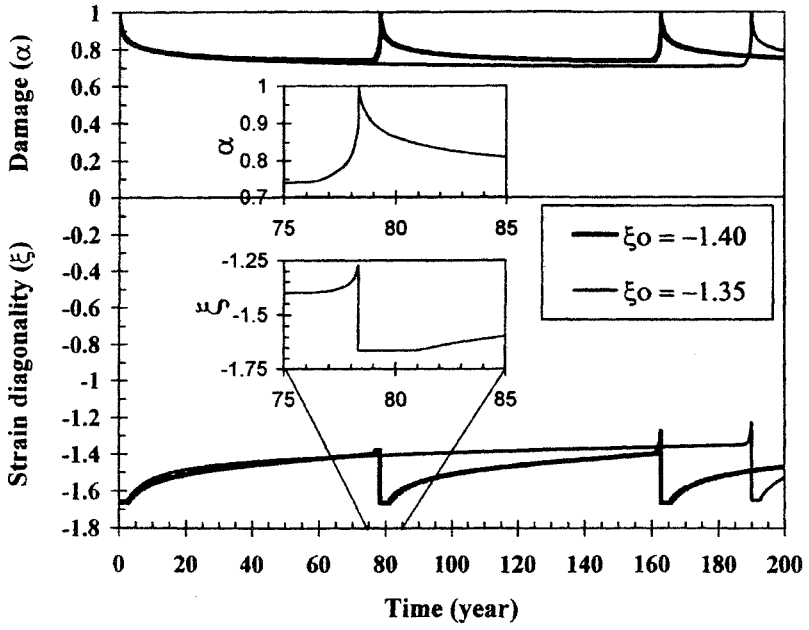

Figure 5. Strain diagonality (ξ) and damage (α) evolution during earthquake cycle for a single fault model. Insert shows ξ and α variations before and after a seismic event. With increase of the critical strain diagonality (ξ_0) from −1.40 to −1.35 the length of the cycle increases about twice. Damage rate constants are C_d=0.1 s^{-1}; C_f=10^{-10} s^{-1}; C_ξ=0.05.

fault system. Since we use the trade-off between fault zone width and ξ_0 to get a realistic average repeat time of large earthquakes, we expect the results on these issues for earthquakes in the approximate magnitude range $6.0 \le M \le 8.5$ not to be affected significantly by the grid size choice.

The interseismic period ends and the preseismic period begins when the current strain diagonality achieves a critical value for "subcritical" crack growth. The condition for damage onset ($\xi > \xi_0$) is satisfied and the damage begins to increase. Increasing damage leads to higher strain and further damage localization since the elastic moduli explicitly depend on the damage variable α as discussed by *Lyakhovsky et al.* [1997a]. In addition, for our elastic upper crust governed by damage rheology, the temporal derivative of stress in equations (13) and (A4) includes a term of a type $\partial\sigma/\partial\alpha \cdot d\alpha/dt$ that implicitly decreases the effective material stiffness for increasing damage. The process of material weakening and increasing preseismic deformation is localized in a small region (one numerical element), and for a grid size that represents realistic fault zone width (e.g., order 100 m or less) this "nucleation" process is not expected to produce an observable surface geodetic signal. The preseismic period ends when the localized damage reaches a critical value for brittle failure. The duration of this period depends on a damage rate coefficient C_d. This is set here as C_d=0.3-0.5 s^{-1}, a value which is somewhat below those (0.5-5 s^{-1}) estimated from laboratory data [*Lyakhovsky et al.*, 1997a], to increase the stability of the numerical procedure. This slightly enlarges the duration of the nucleation weakening period that ends (Figure 5) with initiation of dynamic rupture when α achieves its critical value ($\alpha=\alpha_{cr}$). At the present modeling level we do not simulate details of the dynamic failure process and use a quasi-static solution. However, we introduce a quasi-dynamic procedure for rupture front propagation by recalculating the stress field after a stress drop in every numerical element and by incorporating a dynamic weakening of material everywhere via reduction of the critical value of the damage parameter to $\alpha_{dynamic}$ given by

$$\alpha_{dynamic} = \alpha_{cr} - \sqrt{\tau_r \frac{d\alpha}{dt}} \qquad (15)$$

where τ_r is relaxation time given by the ratio of the effective viscosity of the damaged crust to its rigidity. The effective viscosity is moderated by the rate of damage accumulation and depends on the model structure in a manner similar to that described above. For the numerical simulations shown below we vary τ_r between 10^{-2} and 1 year. Detailed derivation and implications of (15) are discussed by A. Agnon et al. (manuscript in preparation). For infinite viscosity the dynamic weakening (15) implies an ideal brittle behavior. In the initial set of calculations for a single fault model the parameter τ_r is set unrealistically big, so every nucleation of a brittle failure event in some part of the damage zone propagates through the entire area. This leads to relatively simple failure histories consisting of system-sized events occurring in a single fault zone. In section 3.2 we use smaller values of τ_r allowing for the arrest of the rupture front in regions where the preexisting damage is not high enough. The role of this parameter will be explored further in section 3.2 dealing with distributed faulting.

As mentioned earlier, the brittle failure process is set here to drop initially the deviatoric stresses in the rupture zone to zero and to conserve only the volumetric stress. This stress drop produces coseismic displacements in the surrounding material and nonreversible plastic strain in the rupture zone. The latter is modeled in simpler traditional frameworks as slip on a planar fault surface. The amount of plastic strain in the damage zone is related to the total amount of slip deficit during an earthquake cycle. The magnitude of the simulated earthquake may be estimated from the known stress drop or the accumulated plastic strain. Following *Madariaga* [1979], the tensor of the seismic moment (M_{ij}) is a volumetric integral of the stress drop

$$M_{ij} = \int_V \Delta\sigma_{ij} dv \qquad (16a)$$

where V is the volume of the zone sustaining the stress drop ($\Delta\sigma_{ij}$). This relation is more general than the usual definition of the seismic moment

$$M_{ij} = \int_V C_{ijkl} \Delta\varepsilon_{kl}^{(plastic)} dv \qquad (16b)$$

where C_{ijkl} is the tensor of elastic moduli. Unfortunately, stress drop determinations are subjected to large uncertainties, and it is not possible in practice to obtain $\Delta\sigma_{ij}$ through the failure zone. Another option is to calculate the potency [*Ben-Menahem* and *Singh*, 1981] of the event as

$$P_{ij} = \int_V \Delta\varepsilon_{kl}^{(plastic)} dv \qquad (17)$$

Heaton and Heaton [1989], *Ben-Zion* [1989] and *Amelung and King* [1997] argued that the potency provides a better physical measure of the overall size of an earthquake than the seismic moment. In general, routine processing of seismograms for seismic moment (the zero spectral asymptote) provides no information on material properties, and the rigidity part of the moment is assumed rather than being derived from the data. Furthermore, the inclusion of rigidity in the definition of the seismic moment makes it ambiguously defined for the general case of laterally heterogeneous fault zones. For simple cases of constant elastic properties the potency, also referred to as geometric moment [*Kanamori* and *Anderson*, 1975], is equal to the seismic moment divided by rigidity. However, for the more realistic case discussed here, this simple relation does not hold a priori since the elastic properties evolve very strongly during the earthquake rupture process. The relation between moment and potency in our model with variable rigidity is not unique, and we analyze it with results based on the distributed damage model of section 3.2. We calculate the earthquake magnitudes in two ways: (1) from the seismic moment (16a) using the empirical relation $M=2/3[\log_{10}(M_0)-16.1]$, where $M_0=(M_{ij}M_{ij})^{1/2}$ is moment in dyne cm [*Hanks and Kanamori*, 1979], and (2) from the potency using the empirical relation $M=(2/3)\log_{10}(P)+3.6$, where $P=(P_{ij}P_{ij})^{1/2}$ is in km^2 cm [*Ben-Zion and Rice*, 1993].

Figure 6 shows a good correlation between event magnitudes in the model with distributed damage (see section 3.2) calculated in these two different ways. Note that we used the moment definition (16a) that does not include explicitly material properties, rather than the relation usually used by seismologists to derive seismic moment from data, (16b) or its Fourier transform. The relation (16b) contains material properties and does not have a unique well-defined meaning for deformation process involving spatio temporal changes of elastic moduli studied here and presumably occurring during earthquakes.

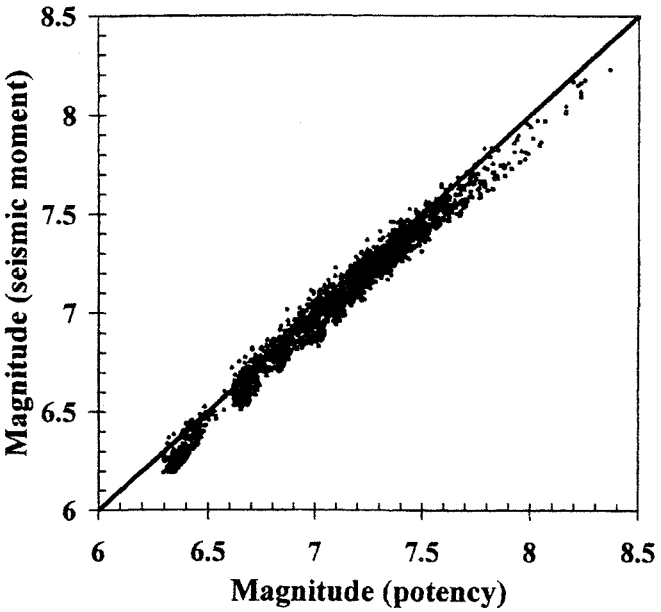

Figure 6. Correlation between earthquake magnitudes calculated using seismic moment and potency based on model runs with different parameters.

In contrast to rupture nucleation, material healing after the seismic event occurs in the whole rupture zone simultaneously during the postseismic period. The same term $\partial\sigma/\partial\alpha \cdot d\alpha/dt$ that was responsible for stiffness reduction during the preseismic period reverses its sign and locks the damage zone by increasing the effective rigidity. This produces rapid transient strengthening that is followed by actual material healing (i.e., decrease of damage). This temporarily prevents an increase of the strain diagonality during a few years after the event (Figure 5) when the damage level is still very high. The characteristic time scale for material healing depends on values of the coefficients C_1, C_2 in the equation for healing in the damage rheology model [*Lyakhovsky et al.*, 1997a, equation 42]. Figure 7 shows the decrease of damage due to confining pressure during 3 years of the postseismic period for three different pairs (C_1, C_2) used in the simulations and referred to as fast, medium and slow. The material recovers 20-30% of its damage-free rigidity to α=0.7-0.8 during the first half a year for all the cases. After that, the healing rate significantly decreases, and total recovery after 3 years of the postseismic period approaches 30-50% (α=0.5-0.7). The most active period of locking of the damage zone is around half a year. This time scale is comparable with that reported by *Savage and Svarc* [1997] based on postseismic deformation associated with the 1992 Landers earthquakes and by *Zhao et al.* [1997] based on inferred states of stress before and after the 1994 Northridge earthquake. The rate and level of material recovery do not significantly change the behavior of a single fault model, but they govern the style of strain localization and earthquake statistics in the model with distributed faulting discussed in section 3.2.

3.2. Regional Earthquakes and Fault Networks

The following simulations are aimed at the study of the process of damage-strain localization, evolution of fault networks, and statistics of simulated seismic events. We start each simulation with randomly distributed damage (and hence stiffness) such that the stress and strain are in equilibrium. Instead of the localized step function velocity of the upper mantle, employed in section 3.1, we use a linear velocity profile at the base of the substrate. The values of the base velocities on the left and right edges are equal to those used for the single-fault model. All material properties except those responsible for the kinetics of the damage process are the same as in the single-fault model.

The ratio between the rate of healing and the rate of loading is central to the model behavior. It controls the style of localization and type of earthquake statistics. We define the loading timescale, τ_L, as the time needed to reaccumulate (rebuild) the elastic shear strain from a stress drop of a brittle failure to a level that gives strain ratio ξ equal to the critical value (ξ_0=−1.35). This loading timescale depends on the relaxation time of the viscoelastic system of upper and lower crust layer (Figure 2), and the amplitude of the imposed mantle motion. The healing time scale, τ_h, characterizes the rock memory, or how long a material that is broken in a seismic event stays significantly weaker than its unbroken surrounding. This value depends on confining pressure and healing rate coefficients (Figure 7). In the following set of simulations we keep the loading timescale constant and vary the healing rate coefficients.

The first set of simulations corresponds to slow healing (solid line in Figure 7). The geometry of the high damage zone formed by the first few events reflects the initial random distribution and keeps its overall geometrical features during more than a thousand model years. Most of the seismic events occur in the same zone and occupy a similar volume. The slip accumulates in a relatively narrow and regular damage zone (Figure 8 and Plate 1 on the left) and preserves some features of the initial random damage for a long period. This behavior leads to a preferred event size manifested as a narrow local maximum in noncumulative frequency-size statistics of model earthquakes. We refer here to such statistics with a preferred event size as characteristic

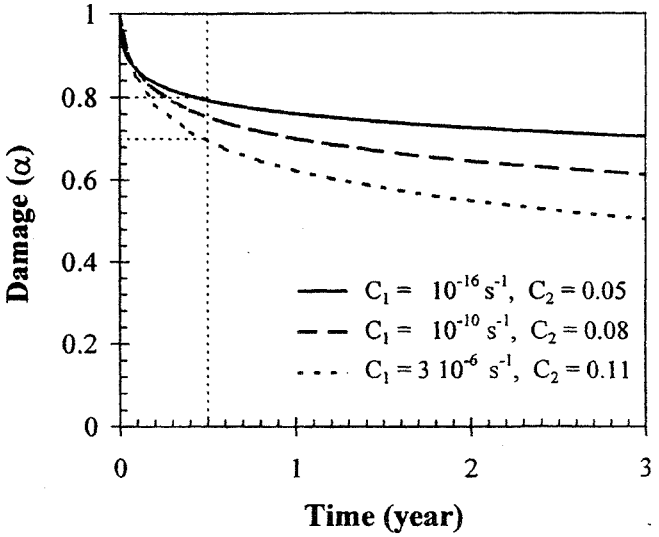

Figure 7. Material recovering (damage versus time) under constant lithostatic pressure and zero shear stress. Three different sets for healing rate constants represent slow, medium, and fast healing.

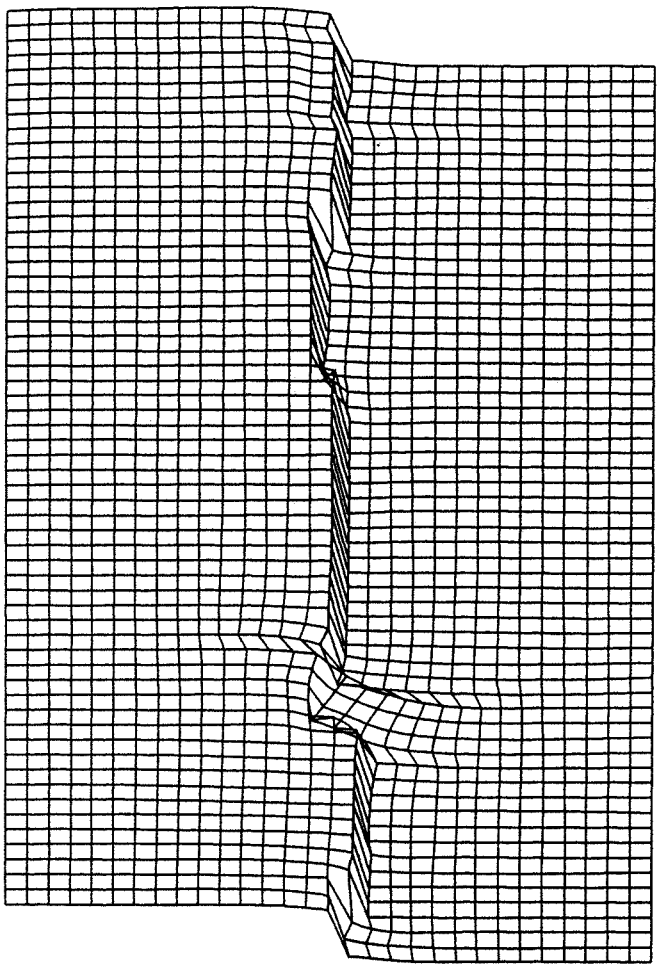

Figure 8. Typical distribution of the cumulative strain for the model with slow healing. The slip and high damaged material (Plate 1 on the left) are concentrated in relatively narrow and regular zone.

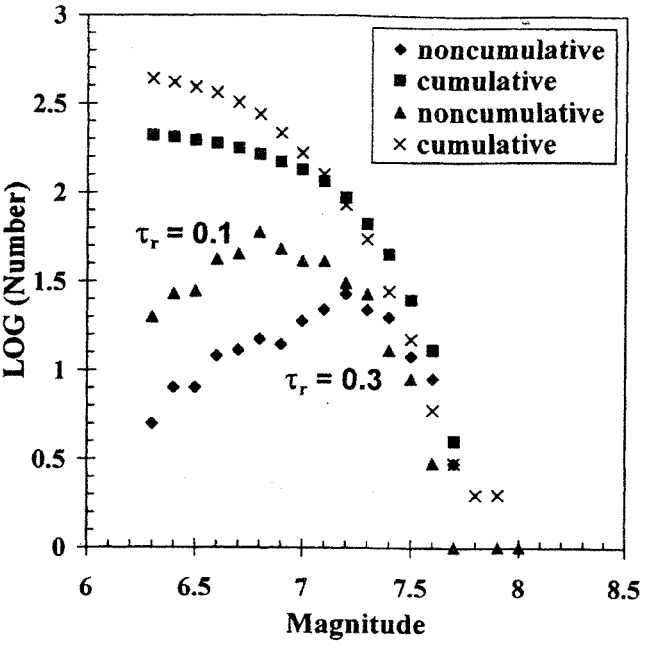

Figure 9. Cumulative and noncumulative frequency-size statistics of seismic events for slow damage healing (long material memory) and different τ_r. The statistics have a preferred event size manifested as a narrow local maximum in the noncumulative distribution.

earthquake distribution. The magnitude of the characteristic events strongly depends on the prescribed dynamic weakening. Relatively small values (τ_r=0.1 year) give a maximum in the non-cumulative statistics for earthquakes with magnitude from 6.7 to 6.9 (Figure 9). Relatively large values of the dynamic weakening (τ_r=0.3 year) shift the maximum to event magnitude of ~7.2-7.4 without changing the form of the statistics.

Increasing of the material recovering (dashed line in Figure 7) leads to broadening of the maximum in the non-cumulative frequency-size statistics (Figure 10), changing it towards a Gutenberg-Richter power law distribution. The cumulative number of events with magnitude larger 7.2 could be approximated by a linear relation with b=2.5, a value significantly larger than the observed b value near unity. Further small increasing of the material recovering (dotted line in Figure 7) significantly increases the geometrical complexity of the evolving damage zones (Figure 11 and Plate 1 on the right). The large conjugate structures accumulate significant amount of displacement. The offsets between fault segments increase, and some of them produce branching that prohibits their further propagation. Part of the simulated region can preserve distributed damage (Plate 1) without being involved in the process of damage localization for a long time. The frequency-size earthquake statistics for the fast healing case are much closer to the Gutenberg-Richter distribution. A linear relation with b=1.3 can approximate the

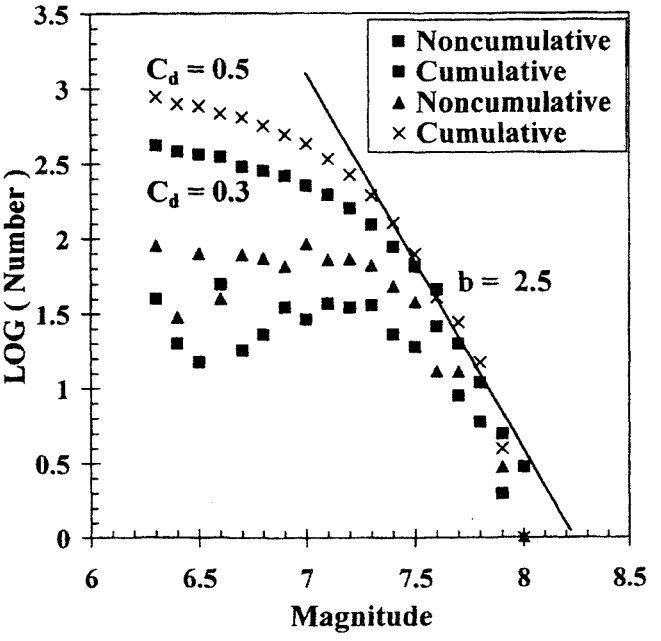

Figure 10. Frequency-size statistics of seismic events for medium damage healing and different damage rate constants C_d. The cumulative number of large events may be approximated by a linear relation with b=2.5, a value significantly larger than typically observed b values near unity.

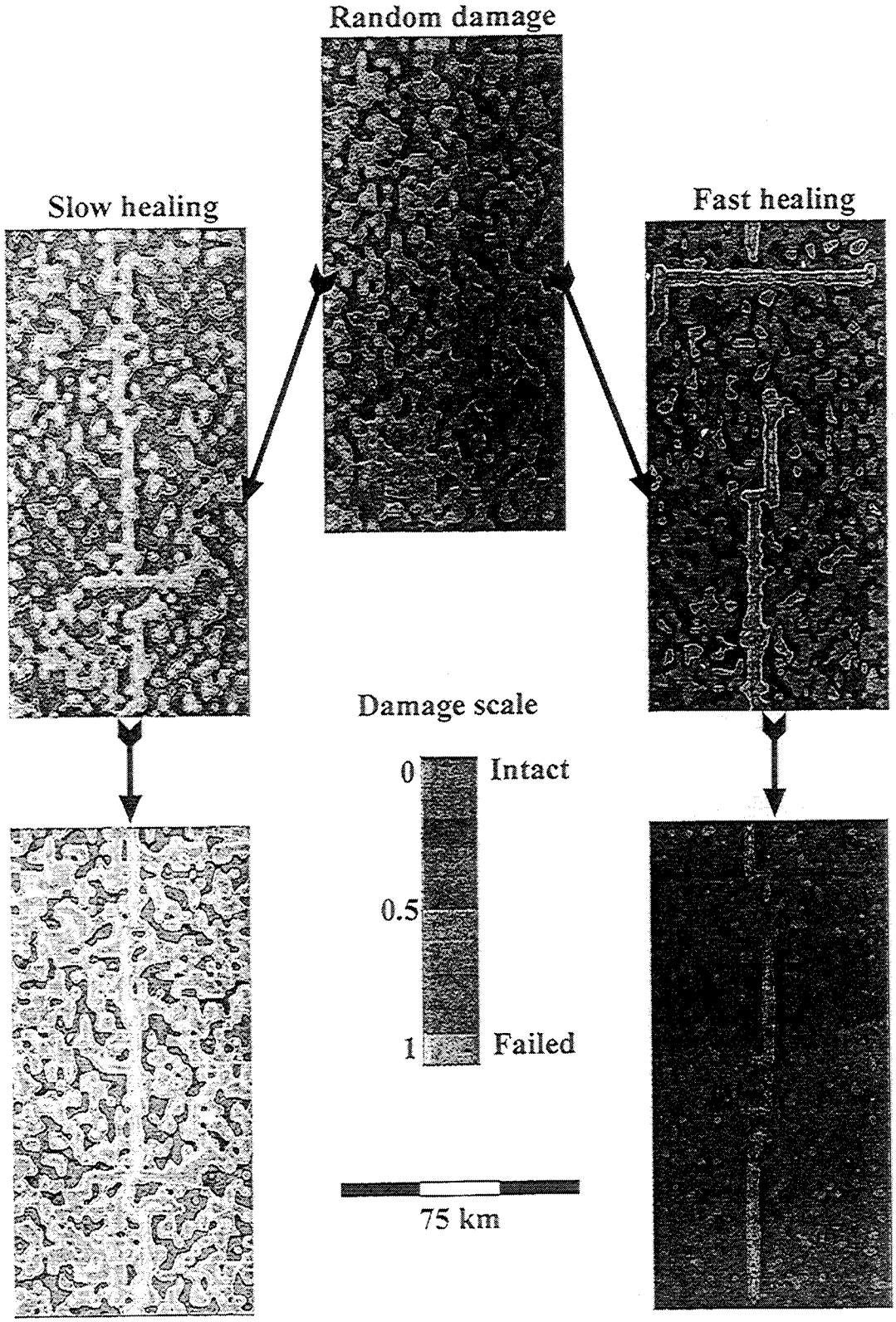

Plate 1. Typical patterns of damage distribution and its evolution for (left) a model with slow healing, and (right) a model with fast healing.

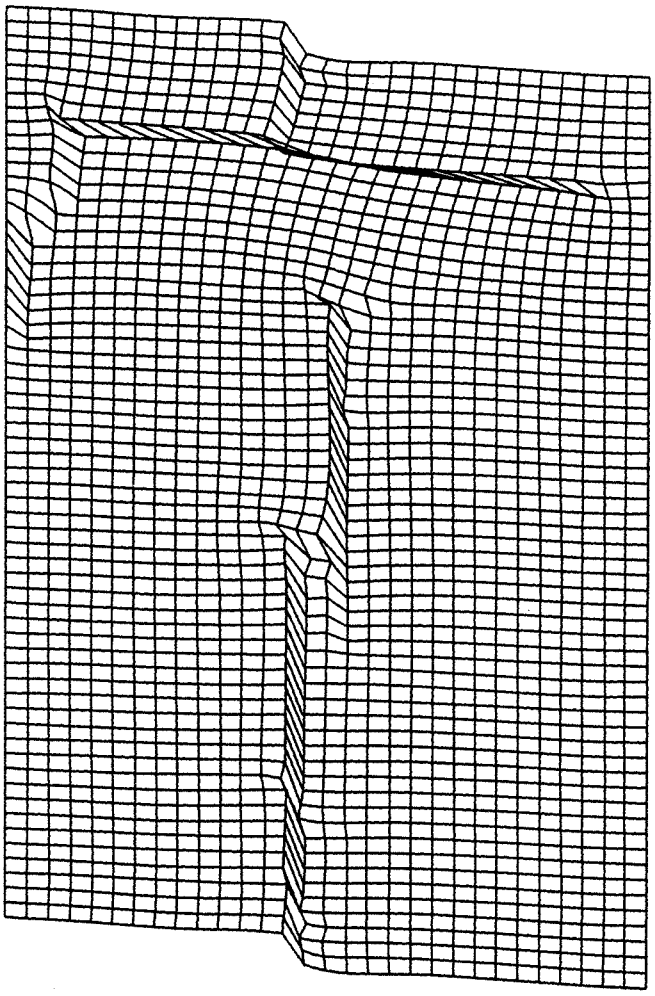

Figure 11. Cumulative strain for a model with fast healing. Large conjugate structures accommodate significant amount of displacement.

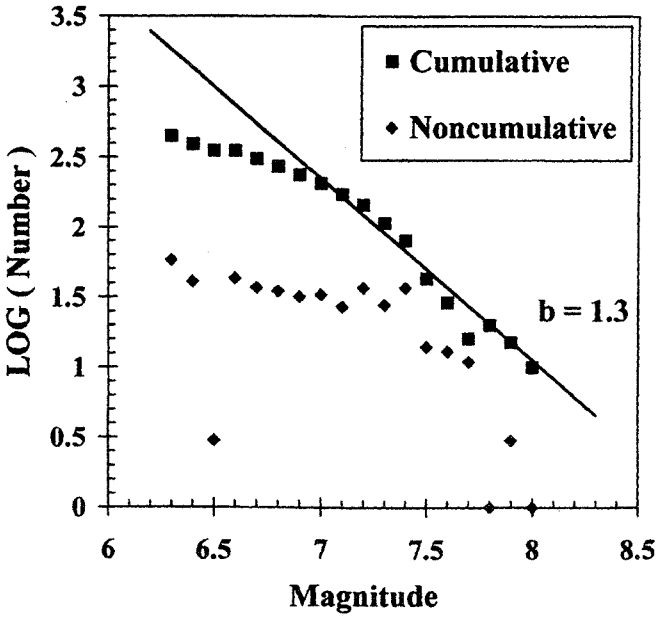

Figure 12. Frequency-size statistics of seismic events for fast damage healing. A linear relation with b=1.3 can approximate the cumulative statistics of events with magnitude larger 6.8.

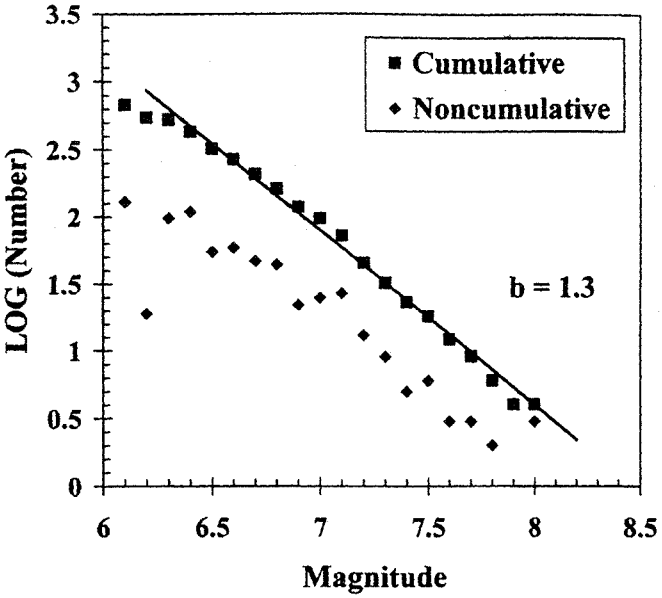

Figure 13. Frequency-size statistics of seismic events for fast damage healing and small spatial variations of material strength. The statistics are compatible with the Gutenberg-Richter power law distribution for the entire simulated magnitude range (compare with Figure 12).

cumulative statistics of events with magnitude larger 6.8 (Figure 12). If the crust properties other than damage are perfectly homogeneous, the geometrical complexity of the fault system (Figure 11 and Plate 1 on the right) is not preserved during a period of many earthquake cycles. In this case a broad damage zone has a tendency to collapse into a narrow one similar to that shown in Figure 8 and Plate 1 on the left, sustaining characteristic earthquakes that produce deviation from the Gutenberg-Richter distribution for events with magnitude 7.0-7.3. The situation is, however, different for a slightly heterogeneous crust. Even small spatial variations in material parameters representing the strength of the upper crust as critical strain diagonality (ξ_0) or dynamic weakening (τ_r) or both prevent the foregoing regularization tendency and lead to fault zones with sustained geometrical complexities. The corresponding frequency-size statistics follow a power law with b=1.3 (Figure 13) for the entire simulated magnitude range. This value falls in the range of the observed b=0.7-1.35 in regional and global earthquake catalogs [*Frohlich and Davis*, 1993].

In such cases we also find that the seismic response of the model (Figure 14) exhibits long-term fluctuations that we have called "mode switching" activity [*Ben-Zion et al.*, 1999b]. The temporal evolution of seismicity switches back and forth between intervals with clusters of intense seismic activity lasting several large earthquake cycles and relatively quiet intervals of similar duration. Most earthquakes in the relatively active intervals have magnitudes above 6.8, and the frequency-size statistics in these portions of the response are compatible with the characteristic earthquake distribution. During the relatively quiet periods the event magnitudes are below M=6.8, and the frequency-size statistics are compatible with a truncated power law. The earthquake sequences before and after the largest model events (Figure 14, insets) show diverse patterns. The largest earthquake in the left inset is surrounded by a cluster of strong events, while the largest

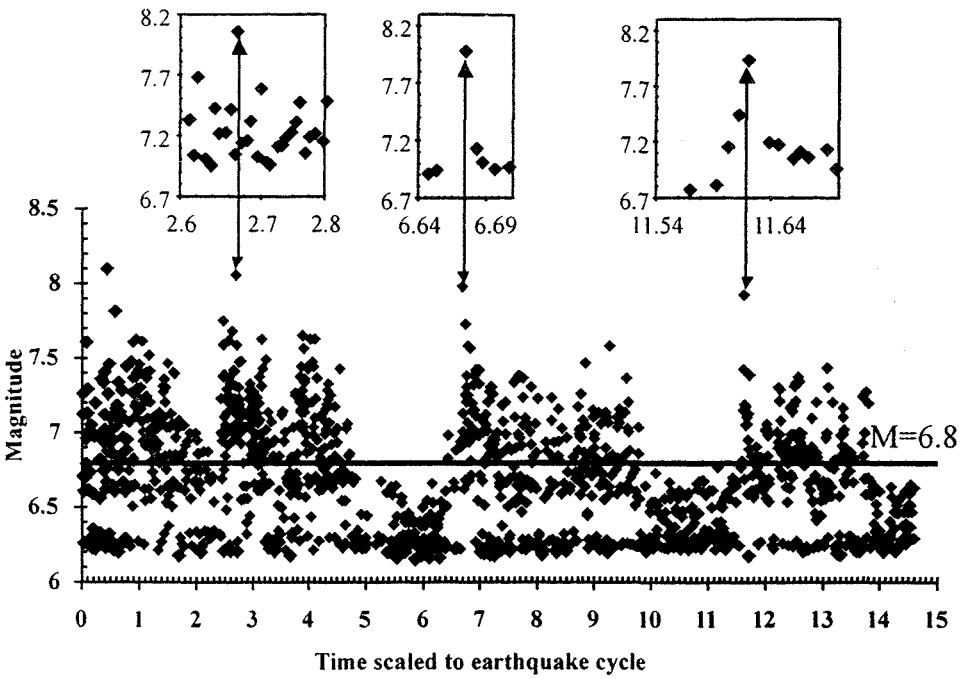

Figure 14. Seismicity record with mode-switching activity, consisting of time intervals of several large earthquake cycles with clusters of large events, separated by intervals of similar duration with only small and intermediate size earthquakes. The insets show a variety of different event sequences before and after the largest model earthquakes.

events in the middle and right insets have narrow and wide foreshock and aftershock sequences, respectively. If the material recovery is increased further, so that effective healing occurs in a small fraction of a large earthquake cycle, the behavior changes from mode switching to sustained response with disordered networks of faults and frequency-size statistics compatible with the Gutenberg-Richter distribution [*Ben-Zion et al.*, 1999b].

4. Discussion

We introduce a nonlinear continuum mechanics framework for simulating the coupled evolution of earthquakes and faults in a regional model consisting of a seismogenic upper crust governed by damage rheology over a layered viscoelastic half-space. The damage rheology [*Lyakhovsky et al.*, 1997a] incorporates nonlinear and irreversible aspects of rock deformation, including localization and nucleation phases, strength evolution with slip and time, and branching from the main rupture plane. The model accounts for interactions between evolving fault zones, and interaction of the brittle seismogenic crust with a viscoelastic substrate. The results illustrate the importance of four different timescales for the evolution of the crust and frequency-size earthquake statistics.

Our previous analysis [*Lyakhovsky et al.*, 1997a] focused on three of the controlling timescales. One for degradation, τ_d, is the inverse of the modulus degradation rate and characterizes the duration of the period between damage onset and brittle failure. The second one for loading, τ_l, is the inverse of the total strain rate and characterizes the time needed to reaccumulate the elastic strain from a stress drop of a brittle failure to the critical level for onset of damage. The duration of the earthquake cycle in a single fault model is equal to the sum of τ_d and τ_l. The third timescale, τ_r, comes from the Maxwell relaxation of elastic stresses and is equal to the viscosity divided by rigidity. The dynamic weakening (15) depends on the value of τ_r and thus controls the preferred event size for the characteristic frequency-size distribution. The present work highlights the role of an additional timescale, the healing time τ_h, controlling fault pattern evolution and earthquake statistics in the model for the crust-mantle system [see also *Ben-Zion et al.*, 1999b].

Lyakhovsky et al. [1997a] show a stick-slip cycle with three stages: degradation, instability, and healing. These stages correspond to the interseismic, coseismic, and postseismic stages of a seismic cycle, respectively. The existence of a fourth preseismic stage is indicated by the analysis of localization in a degradable and purely elastic one-dimensional material [*Lyakhovsky et al.*, 1997a]. The localization is also anticipated in a degradable viscoelastic medium if the loading is faster than the viscous relaxation of elastic stress in the undamaged medium ($\tau_r > \tau_l$). A. Agnon et al. (manuscript in preparation) further show that once the degradation is faster than the relaxation ($\tau_r > \tau_d$), the preseismic equivalent stage of subcritical crack growth is terminated and a dynamic stress drop ensues. These results are similar to a transition from quasi-static nucleation phase to dynamic rupture in rate- and state-dependent [e.g., *Okubo*, 1989; *Dieterich*, 1992; *Ben-Zion and Rice*, 1997] and slip-weakening [*Shibazaki and Matsu'ura*, 1992; *Ohnaka*, 1996] frictional frameworks.

The full four stages in the seismic cycle are manifested in the present model. The model provides an improvement over the generalized Elsasser model [*Li and Rice*, 1987] in simulating geodetic signals with algebraic decay compatible with observations, close to the fault as well as in the far field. The calculated velocity profile for the fault parallel velocity fits well an arctangent curve (Figure 4) that represents the average geodetic measurements for the middle part of the earthquake cycle, all the way to the fault zone. During the

preseismic stage the elastic degradation is localized in a small area (one numerical element) and does not produce a significant geodetic signal. The dynamic weakening (15) and the proper 3-D elastic stress transfer calculated using the Green function (14) allow a failure in a hypocenter to extend into a region with possible complex geometry. The high healing rate in the postseismic period increases the effective rigidity across the fault zone. The corresponding healing time-scale, τ_h, is comparable to that reported by *Savage and Svarc* [1997] based on postseismic deformation following the 1992 Landers earthquakes and by *Zhao et al.* [1997] based on inferred states of stress before and after the 1994 Northridge earthquake.

Ben-Zion and Rice [1993, 1995] and *Ben-Zion* [1996] simulated seismicity patterns along a strike-slip fault with fixed prescribed heterogeneities. Their models represent approximately geometric disorder of a narrow fault zone by various types of disorder in strength properties. The simulations of the present work allow us to compare results from evolving complex structures with true geometric disorder to the simple planar approximations of Ben-Zion and Rice. In our model, the ratio between the time-scales of healing and loading (τ_h/τ_l) provides a guideline for understanding different dynamic regimes of fault pattern evolution and earthquake statistics that are evident in the simulations (Figures 8-14 and Plate 1). When the system has long-term memory (τ_h/τ_l is relatively high), it produces fast damage localization during a time interval less than one large earthquake cycle. This leads to the development of geometrically regular fault systems and frequency-size event statistics compatible with the characteristic earthquake distribution. In such cases, the event statistics are similar to those simulated by model realizations of *Ben-Zion and Rice* [1993, 1995] and *Ben-Zion* [1996] with relatively regular heterogeneities. Conversely, if the memory of the system is short-term (τ_h/τ_l is relatively low), it develops highly disordered fault systems and produces power law frequency-size statistics compatible with the Gutenberg-Richter distribution. In these cases, the event statistics are similar to those simulated by model realizations of Ben-Zion and Rice with highly disordered heterogeneities. The correlation between fault complexity and frequency-size statistics suggested by the present model and the previous simulations of *Ben-Zion and Rice* [1993, 1995] and *Ben-Zion* [1996] is in agreement with field and seismological observations of *Wesnousky* [1994] and *Stirling et al.* [1996].

For intermediate ratio of timescales τ_h/τ_l, the results exhibit switching of response between two distinct modes of activity (Figure 14). The first mode is associated with clusters of large earthquakes and frequency-size statistics compatible with the characteristic earthquake distribution, while the second mode is characterized by relatively low moment/potency release and frequency-size event statistics following a truncated power law. The average duration of each activity mode scales with the time interval of a large earthquake cycle in the system. As discussed by *Ben-Zion et al.* [1999b] and *Dahmen et al.* [1998], similar activity switching exists for a range of parameters in the simpler planar models of *Ben-Zion and Rice* [1993, 1995]. Long-term switching of seismic activity between relatively active and relatively quiet time intervals has been indicated by disturbed sediments and surface faulting in the Dead Sea transform, in a continuous record spanning 50 thousand years [*Marco et al.*, 1996]. Qualitatively similar alternating deformation phases have been documented in the eastern California Shear Zone [*Rockwell et al.*, 2000], the Great Basin Province in the western United States [*Wallace*, 1987], the Loreto basin, Baja California [*Dorsey et al.*, 1997], and other locations summarized by *Ben-Zion et al.* [1999b]. In the Dead Sea transform sites studied by *Marco et al.* [1996], each active period may exceed 10,000 years and contain up to 15 large events, sevenfold to tenfold more than in the relatively quiet periods. A similar picture would emerge from Figure 14 for events with $M>7.5$. The first half of the record shows a cluster with 17 $M>7.5$ events, whereas the second shows only 4 events. The scaling of this model to the Dead Sea transform should account for an order of magnitude lower loading rate [*Joffe and Garfunkel*, 1987; *Ellenblum et al.*, 1998; *Pe'eri et al.*, 1999].

Our simulated event statistics depend in general on the space-time window of the observational domain; that is, temporal sequences from different regions are not statistically equivalent among themselves, nor are they statistically equivalent to spatial ensembles of earthquakes occurring in different zones. The results imply that extrapolations of observed earthquake statistics based on low-magnitude seismicity and short time intervals to large earthquake behavior over longer duration require careful justification tailored to the particular case in hand.

Appendix A: Damage Mechanics

The macroscopic effects of distributed cracking and other types of damage require treatment by constitutive models that include nonlinear stress-strain relations together with material degradation and recovery. In order to simulate a process of fracturing in terms of continuum mechanics, a nondimensional intensive damage variable α is introduced. The variable α is related to the density of microcracks in a laboratory specimen, or the density of small faults in a crustal domain. For the sensitivity of elasticity to distributed cracks, consider the response of a single crack. Across the crack there is no cohesion, so under extension the crack dilates, diminishing the resistance to loading. Conversely, under normal pressure, contact forces across the crack resist deformation. *Lyakhovsky et al.* [1997b] derive the macroscopic stress-strain relations for a 3-D elastic solid accounting for the cumulative effect of microcrack opening and closure and test the solution against rockmechanics experiments. Following their formulation the elastic potential is written as

$$U=\frac{1}{\rho}\left(\frac{\lambda}{2}I_1^2+\mu I_2-\gamma I_1\sqrt{I_2}\right) \qquad \text{(A1)}$$

where λ and μ are Lame constants, $I_1=\varepsilon_{kk}$ and $I_2=\varepsilon_{ij}\varepsilon_{ij}$ are two independent invariants of the strain tensor ε_{ij}, and γ is an additional elastic modulus (summation notation is assumed). The second order term with the new modulus γ accounts for microcrack opening and closure in a damaged material. The term incorporates nonlinear elasticity even for an infinitesimal strain, and it simulates abrupt change in the elastic properties when the loading reverses from compression to tension. The stress tensor σ_{ij} derived from (A1) is

$$\sigma_{ij}=\left(\lambda-\gamma\frac{\sqrt{I_2}}{I_1}\right)I_1\delta_{ij}+\left(2\mu-\gamma\frac{I_1}{\sqrt{I_2}}\right)\varepsilon_{ij} \qquad \text{(A2)}$$

The stress-strain relation (A2) can be rewritten to mimic the usual form of Hook's law by introducing effective elastic moduli

$$\lambda^e = \lambda - \frac{\gamma}{\xi}; \quad \mu^e = \mu - \frac{1}{2}\gamma\xi \tag{A3}$$

where the strain diagonality $\xi = I_1/\sqrt{I_2}$ characterizes the type of deformation. *Agnon and Lyakhovsky* [1995] suggested that the elastic moduli μ and γ are linear functions of the damage α and chose only the modulus λ to be constant:

$$\lambda = \lambda_0 = const; \quad \mu = \mu_0 + \alpha\xi_0\gamma_r; \quad \gamma = \alpha\gamma_r \tag{A4}$$

where γ_r is calculated from the conditions [*Lyakhovsky et al.*, 1997a, equations (14) and (15)] of convexity loss for the maximum value of the damage variable (α=1). They also related the critical strain diagonality (ξ_0) to the friction angle φ by considering the critical shear stress for Mohr-Coulomb sliding:

$$\tau = \tan(\varphi)\sigma_n \tag{A5}$$

where σ_n is normal stress. Consider a saw-cut interface between two intact blocks in a friction experiment carried out under confining pressure. The condition for fault slip is then [*Agnon and Lyakhovsky*, 1995]

$$\xi_0 = \frac{-\sqrt{3}}{\sqrt{2q^2(\lambda_0/\mu_0 + 2/3)^2 + 1}} \tag{A6}$$

where q=sin(φ)/[1−sin(φ)/3]. Physically, (A6) means that the critical strain diagonality ξ_0 is some modification of the internal friction. *Savage et al.* [1996] draw a connection between macroscopic friction measured on saw-cut specimens and internal friction that characterizes shear fracture of intact rock. They write the strength of an intact rock as the sum over the plane of the incipient fault of both friction on closed microcracks and strength of the remaining grains. The approach taken by damage mechanics [*Lyakhovsky et al.*, 1997a] extends that connection. Under confining pressures sufficient for closure of microcracks, stress concentration may arise only once the shear stress meets the frictional criterion. Then favorably oriented cracks slide and load their tips giving rise to damage increase. The difference between the frictional strength of prefaulted surfaces and the strength of the intact rock is given by the excess stress that is needed to increase the damage from its initial value to critical. That stress difference is rate-dependent, and it can be calculated readily from the model damage kinetic equations:

$$\frac{d\alpha}{dt} = C \cdot I_2(\xi - \xi_0), \tag{A7}$$

where C depends on ξ and α (see *Lyakhovsky et al.* [1997a] for thermodynamic derivations and more details).

Appendix B: Numerical Scheme

The system of equations that should be solved numerically consists of the equation of motion of the hybrid model and equations describing damage evolution and transient stress redistribution. Here we rewrite all these equations with brief comments on the numerical approach to their solution. We start with the equation of motion (13)

$$H\iint_S G_{kn}\frac{\partial}{\partial t}\frac{\partial\sigma_{nm}}{\partial x_m}ds + \frac{Hh}{\eta}\frac{\partial\sigma_{km}}{\partial x_m} = \frac{\partial u_k}{\partial t} - V^{(k)}_{plate} \tag{B1}$$

which is solved by iterative procedure similar to "FLAC" [*Cundall and Board*, 1988]. For the known elastic strain and all material parameters from the previous time step an iterative procedure gives new velocities ($V_i=\partial u_i/\partial t$) in the simulated area. The computational Lagrangian mesh consists of quadrilateral elements, which are subdivided into pairs of constant strain triangles, with different diagonals. This double overlay scheme ensures symmetry of the solution by averaging results obtained on two meshes. Linear triangular element shape functions L_k (k=1,3) are defined as

$$L_k = a_k + xb_k + yc_k \tag{B2}$$

where a_k, b_k, and c_k are constants and (x, y) are grid coordinates. These shape functions are used to interpolate the nodal velocities $v_i^{(k)}$ within each triangle element:
defined as

$$v_i(x,y) = \sum_{k=1}^{3} v_i^{(k)} L_k \tag{B3}$$

Equation (B3) enables calculation of the strain rate tensor e_{ij} in each triangle. The stress tensor σ_{ij} is calculated using elastic deformation, ε_{ij}, from the previous time step according to nonlinear stress-strain elastic relations [*Lyakhovsky et al.*, 1997b]. Being partially differentiated respect to time coordinate, equation (A2) gives the relation between $\partial\sigma_{ij}/\partial t$ and strain rate tensor e_{ij}:

$$\begin{aligned}\frac{\partial\sigma_{11}}{\partial t} &= \lambda e_{11} - \gamma\frac{\varepsilon_{11}e_{11} + \varepsilon_{22}e_{22} + 2\varepsilon_{12}e_{12}}{\sqrt{I_2}} \\ &- \gamma\varepsilon_{11}\left[\frac{e_{11}+e_{22}}{\sqrt{I_2}} - \xi\frac{\varepsilon_{11}e_{11} + \varepsilon_{22}e_{22} + 2\varepsilon_{12}e_{12}}{I_2}\right] \\ &+ (2\mu - \gamma\xi)e_{11} + \frac{d\lambda}{dt}I_1 - \frac{d\gamma}{dt}\sqrt{I_2} \\ &+ \left(2\frac{d\mu}{dt} - \frac{d\gamma}{dt}\xi\right)\varepsilon_{11}\end{aligned} \tag{B4a}$$

$$\begin{aligned}\frac{\partial\sigma_{22}}{\partial t} &= \lambda e_{22} - \gamma\frac{\varepsilon_{11}e_{11} + \varepsilon_{22}e_{22} + 2\varepsilon_{12}e_{12}}{\sqrt{I_2}} \\ &- \gamma\varepsilon_{22}\left[\frac{e_{11}+e_{22}}{\sqrt{I_2}} - \xi\frac{\varepsilon_{11}e_{11} + \varepsilon_{22}e_{22} + 2\varepsilon_{12}e_{12}}{I_2}\right] \\ &+ (2\mu - \gamma\xi)e_{22} + \frac{d\lambda}{dt}I_1 - \frac{d\gamma}{dt}\sqrt{I_2} \\ &+ \left(2\frac{d\mu}{dt} - \frac{d\gamma}{dt}\xi\right)\varepsilon_{22}\end{aligned} \tag{B4b}$$

$$\begin{aligned}\frac{\partial\sigma_{12}}{\partial t} &= (2\mu - \gamma\xi)e_{12} \\ &- \gamma\varepsilon_{12}\left[\frac{e_{11}+e_{22}}{\sqrt{I_2}} - \xi\frac{\varepsilon_{11}e_{11} + \varepsilon_{22}e_{22} + 2\varepsilon_{12}e_{12}}{I_2}\right] \\ &+ \left(2\frac{d\mu}{dt} - \frac{d\gamma}{dt}\xi\right)\varepsilon_{12}\end{aligned} \tag{B4c}$$

When stresses σ_{ij} and their temporal derivation $\partial\sigma_{ij}/\partial t$ are known, the summation on the left side of (B1) results in some vector (F_i) at each node, which is used for calculation of new velocities by simple iterative procedure:

$$v_i^+ = v_i^- + \chi\left(F_i + V_{plate} - v_i^-\right) \tag{B5}$$

The iteration parameter χ provides a convergence of the procedure, which is repeated until the maximum difference between previous v_i^- and next v_i^+ values of velocities become negligibly small. Calculated velocity distribution is used for the Lagrangian transport equation for node coordinates:

$$x_i^+ = x_i^- + v_i dt \tag{B6}$$

and new total strain

$$\varepsilon_{ij}^+ = \varepsilon_{ij}^- + \frac{1}{2}\left(\frac{\partial v_i}{\partial x_j} + \frac{\partial v_j}{\partial x_i}\right)dt \tag{B7}$$

The new z component of elastic strain is defined according to the average lithostatic pressure ($\sigma_{zz}=-\rho gH/2$):

$$\varepsilon_{zz} = -\frac{1}{\lambda^e + 2\mu^e}\left[\lambda^e\left(\varepsilon_{xx} + \varepsilon_{yy}\right) + \rho g\frac{H}{2}\right] \tag{B8}$$

New thickness of the upper crust is calculated using continuity equation ($\mathrm{div}(v_i)=0$) and local isostasy assumption:

$$H^+ = H^-\left[1 - \left(\frac{\partial v_x}{\partial x} + \frac{\partial v_y}{\partial y}\right)dt\right] \tag{B9}$$

New damage distribution is calculated using evolution equation:

$$\alpha^+ = \alpha^- + \left[C_d I_2(\xi - \xi_0)\right]dt \tag{B10a}$$

for degradation ($\xi>\xi_0$), and

$$\alpha^+ = \alpha^- + \left[C_1 \exp\left(\frac{\alpha}{C_2}\right) I_2(\xi - \xi_0)\right]dt \tag{B10b}$$

for healing ($\xi<\xi_0$). The time step dt used for all these numerical procedures is selected after two conditions:

1. Damage change in each time step does not exceed some constant value ($\Delta\alpha_{max}$) selected by comparing a series of similar runs

$$dt_{damage} = \frac{(\Delta\alpha)_{max}}{\left(\frac{d\alpha}{dt}\right)_{max}} \tag{B11}$$

2. Numerical stability of the parabolic equation (B1) based on the Fourier stability analysis requires that the time step Δt is less then half of the relaxation time of the shortest wave length, related to the grid size Δx [*Ames*, 1977]. The upper boundary for the time step used in the simulations is equal to one third of the characteristic time of the attenuation of the wave with length equal to Δx:

$$\Delta t_{max} = \frac{1}{3}\frac{\Delta x^2}{hH\mu/\eta} < \frac{1}{3}\frac{\Delta x^2 + H\mu G_{yy}(\frac{2\pi}{\Delta x})}{hH\mu/\eta} \tag{B12}$$

At some stage of evolution the level of damage in one or several elements achieves the critical level, corrected after the dynamic weakening (15). These elements can not further keep stress, which should be dropped. The immediate change of the stress $\Delta\sigma_{ij}$ is equivalent to distributed force along the element boundary, S, with vector n_k normal to it:

$$F_j = \Delta\sigma_{jk} n_k \tag{B13}$$

and the coseismic elastic displacements are calculated using the Green function (14):

$$u_k^{(e)} = \iint_S G_{kj} F_j ds \tag{B14}$$

The elements involved in the failure process accumulate plastic strain components that are recorded together with the values of the stress drop for calculation of the earthquake moment and potency.

Acknowledgments. We thank Norm Sleep, Bruce Shaw and Ruth Harris for constructive reviews. A. Agnon acknowledges support from the Israel Science Foundation, grant ISF-696/95. V. Lyakhovsky was supported by the Camea Foundation. Y. Ben-Zion was supported by the National Science Foundation (grant EAR-9725358) and the Southern California Earthquake Center (based on NSF cooperative agreement EAR-8920136 and USGS cooperative agreement).

References

Agnon, A., and V. Lyakhovsky, Damage distribution and localization during dyke intrusion, in *Physics and Chemistry of Dykes*, edited by G. Baer and A. Heimann, pp. 65-78, R.A. Balkhema, Brookfield, Vt., 1995.

Amelung, F. and G. King, Earthquake scaling laws for creeping and non-creeping faults, *Geophys. Res. Lett., 24*, 507-510, 1997.

Ames, W.F., *Numerical Methods for Partial Differential Equations*, 365 pp., Academic,San Diego, Calif., 1977.

Andrews, D. J., Coupling of energy between tectonic processes and earthquakes, *J. Geophys. Res., 83*, 2259-2264, 1978.

Andrews, D. J., Mechanics of fault junctions, *J. Geophys. Res.*, 94, 9389-9397, 1989.

Andrews, D.J., and Y. Ben-Zion, Wrinkle-like Slip Pulse on a Fault Between Different Materials, *J. Geophys. Res., 102*, 553-571, 1997.

Anooshehpoor A., and J. N. Brune, Wrinkle-like Weertman pulse at the interface between two blocks of foam rubber with different velocities, *Geophys. Res. Lett., 26*, 2025-2058, 1999.

Ben-Menahem, A., and S. J. Singh, *Seismic Waves and Sources*, Springer-Verlag, New York, 1981.

Ben-Zion, Y., The response of two jointed quarter spaces to *SH* line sources located at the material discontinuity interface, *Geophys. J. Int., 98*, 213-222, 1989.

Ben-Zion, Y., Stress, slip and earthquakes in models of complex single-fault systems incorporating brittle and creep deformations, *J. Geophys. Res., 101*, 5677-5706, 1996.

Ben-Zion, Y., and D. J. Andrews, Properties and implications of dynamic rupture along a material interface, *Bull. Seismol. Soc. Am., 88*, 1085-1094, 1998.

Ben-Zion, Y., and J. R. Rice, Earthquake failure sequences along a cellular fault zone in a three-dimensional elastic solid containing asperity and nonasperity regions, *J. Geophys. Res., 98*, 14,109-14,131, 1993.

Ben-Zion, Y., and J. R. Rice, Slip patterns and earthquake populations along different classes of faults in elastic solids, *J. Geophys. Res., 100*, 12,959-12,983, 1995.

Ben-Zion, Y., and J. R. Rice, Dynamic simulations of slip on a smooth fault in an elastic solid, *J. Geophys. Res., 102*, 17,771-17,784, 1997.

Ben-Zion, Y., J. R. Rice, and R. Dmowska, Interaction of the San Andreas fault creeping segment with adjacent great rupture zones and earthquake recurrence at Parkfield, *J. Geophys. Res., 98*, 2,135-2,144, 1993.

Ben-Zion, Y., C. Sammis, and T. Henyey, Perspectives on the field of physics of earthquakes, *Seismol. Res. Lett., 70*, 428-431, 1999a.

Ben-Zion, Y., K. Dahmen, V. Lyakhovsky, D. Ertas, and A. Agnon, Self-driven mode switching of earthquake activity on a fault system, *Earth Planet. Sci. Lett., 172*, 11-21, 1999b.

Brune J. N., T. L. Henyey, and R. F. Roy, Heat flow, stress and rate of slip along the San Andreas Fault, California, *J. Geophys. Res., 74*, 3821-3827, 1969.

Brune, J. N., S. Brown, and P. A. Johnson, Rupture mechanism and interface separation in foam rubber model of earthquakes: A possible solution to the heat flow paradox and the paradox of large overthrusts, *Tectonophysics, 218*, 59-67, 1993.

Chinnery, M.A., The deformation of the ground around surface faults, *Bull. Seismol. Soc. Am., 51*, 355-372, 1961.

Cowie, P. A., A healing-reloading feedback control on the growth rate of seismogenic faults, *J. Struct. Geol., 20*, 1075-1087, 1998.

Cundall, P. A., and M. Board, A microcomputer program for

modeling large-strain plasticity problems, in *Numerical Methods in Geomechanics. Procedings of 6th International Conference on Numerical Methods in Geomechanics, Innsbruck,* edited by C. Swoboda, pp. 2101-2108. R.A. Balkhema, Brookfield, Vt., 1988.

Dahmen, K., D. Ertas, and Y. Ben-Zion, Gutenberg-Richter and characteristic earthquake behavior in simple mean-field models of heterogeneous faults, *Phys. Rev. E, 58*, 1494-1501, 1998.

Dieterich, J. H., Earthquake nucleation on faults with rate- and state-dependent strength, *Tectonophysics, 211*, 115-134, 1992.

Dorsey, R. J., P. J. Umhoefer, and P. D. Falk, Earthquake clustering inferred from Pliocene Gilbert-type fan deltas in the Loreto basin, Baja California Sur, Mexico, *Geology, 25*, 679-682, 1997.

Ellenblum, R., S. Marco, A. Agnon, T. Rockwell, and A. Boas, A Crusader castle torn apart by the 1202 earthquake, *Geology, 26*, 303-306, 1998.

Elsasser, W.M., Convection and stress propagation in the upper mantle, in *The Application of Modern Physics to the Earth and Planetary Interiors*, edited by S.K. Runcorn, pp. 223-246, Wiley-Interscience, New York, 1969.

England, P.C., and D.P. McKenzie, A thin viscous sheet model for continental deformation. *Geophys. J. R. Astron. Soc. 70*, 295-321, 1982.

Frohlich, C., and S. D. Davis, Teleseismic b values: or, much ado about 1.0, *J. Geophys. Res., 98*, 631-644, 1993.

Fuis, G. S., and W. D. Mooney, Lithospheris structure and tectonics from seismic-refraction and other data, in *The San Andreas Fault System, California,* edited by R. E. Wallace, *U.S. Geol. Surv. Prof. Pap., 1515*, 207-238, 1990.

Gabrielov, A., and W. I. Newman, Seismicity modeling and earthquake prediction: a review, in *Nonlinear Dynamics and Predictability of Geophysical Phenomena, Geophys. Monogr. Ser.*, vol. 83, edited by W.I. Newman et al., pp. 7-13, AGU, Washington, D.C., 1994.

Hanks, T. C., and H. Kanamori, A moment magnitude scale, *J. Geophys. Res., 84*, 2348-2350, 1979.

Harris, R. A., and R. W. Simpson, In the shadow of 1857 - The effect of the great Ft. Tejon earthquake on subsequent earthquakes in southern California, *Geophys. Res. Lett., 23*, 229-232, 1996.

Heaton, T.H., Evidence for and implications of the self-healing pulses of slip in earthquake rupture, *Phys. Earth Planet. Inter., 64*, 1-20, 1990.

Heaton, H.T., and R. E. Heaton, Static deformation from point forces and force couples located in welded elastic Poissonian halfspaces: Implications for seismic moment tensors, *Bull. Seismol. Soc. Am., 79*, 813-841, 1989.

Heimpel, M., and P., Olson, A seismodynamical model of lithosphere deformation: Development of continental and oceanic rift networks, *J. Geophys. Res. 101*, 16,155-16,176, 1996.

Joffe, S., and Z. Garfunkel, Plate kinematics of the circum Red Sea – A re-evaluation, *Tectonophysics, 141*, 5-22, 1987.

Kanamori, H., and D. L. Anderson, Theoretical basis of some empirical relations in seismology, *Bull. Seismol. Soc. Am., 65*, 1073-1095, 1975.

Kasahara, K., *Earthquake Mechanics*, pp. 248, Cambridge Univ. Press, New York, 1981.

King, G., The accommodation of large strains in the upper lithosphere of the Earth and other solids by self-similar fault systems: The geometrical origin of *b*-value, *Pure Appl. Geophys., 121*, 761-814, 1983.

Lachenbruch, A. H., and J. H. Sass, Thermo mechanical aspects of the San Andreas, in *Proceedings, Conference on the Tectonic Problems of the San Andreas Fault System,* edited by R. L. Kovach and A. Nur, *Stanford Univ. Publ. Geol. Sci., 13*, 192-205, 1973.

Landau, L. D., and E. M. Lifshitz, Theory elasticity, 2nd ed., Pergamon, Tarrytown, N.Y., 1970.

Lehner, F. K., V. C. Li, and J. R. Rice, Stress diffusion along rupturing plate boundaries, *J. Geophys. Res., 86*, 6155-6169, 1981.

Li, V. C., and J. R. Rice, Crustal deformation in great California earthquake cycles, *J. Geophys. Res., 92*, 11,533-11,551, 1987.

Lisowski, M., J. C. Savage, and W. H. Prescott, The velocity field along the San Andreas Fault in central and southern California, *J. Geophys. Res., 96*, 8369-8389, 1991.

Lyakhovsky, V., Y. Ben-Zion, and A. Agnon, Distributed damage, faulting, and friction, *J. Geophys. Res., 102*, 27,635-27,649, 1997a.

Lyakhovsky, V., Z. Reches, R. Weinberger and T. E. Scott, Non-linear elastic behavior of damaged rocks, *Geophys. J. Int., 130*, 157-166, 1997b.

Madariaga, R., On the relation between seismic moment and stress drop in the presence of stress and strength heterogeneity, *J. Geophys. Res., 84*, 2243-2250, 1979.

Marco, S., M. Stein, A. Agnon, and H. Ron, Long-term earthquake clustering: A 50,000-year paleoseismic record in the Dead Sea graben, *J. Geophys. Res., 101*, 6179-6191, 1996.

Meisner, R., and J. Strehlau, Limits of stress in continental crusts and their relation to the depth-frequency distribution of shallow earthquakes, *Tectonics, 1*, 79-83, 1982.

Mooney, W. D., G. Laske, and T. G. Masters, CRUST 5.1: A global crustal model at 5° x 5°, *J. Geophys. Res., 103*, 727-747, 1998.

Moore, D. E., and A. D. Lockner, The role of microcracking in shear fracture propagation in granite, *J. Struct. Geol., 17*, 95-114, 1995.

Mora, P., and D. Place, Simulation of the frictional stick-slip insability, *Pure Appl. Geophys., 143*, 61-87, 1994.

Ohnaka, M., Non-uniformity of the constitutive law parameters for shear rupture and quasi-static nucleation to dynamic rupture: A physical model of earthquake generation processes, *Proc. Natl. Acad. Sci. U.S.A., 93*, 3795-3802, 1996.

Okubo, P. G., Dynamic rupture modeling with laboratory- derived constitutive relations, *J. Geophys. Res., 94*, 12,321-12,335, 1989.

Pe'eri, S., S. Wdowinsky, A. Stibelman, N. Bechor, and Y. Bock, Current deformation across the Dead Sea fault as observed from 18 month of continuous GPS monitoring, paper presented at Annual Meeting, Israel Geol. Soc., Eilat, 1999.

Reches, Z., G. Schubert, and C. Anderson, Modeling of periodic great earthquakes on the San Andreas fault: Effects of nonlinear crustal rheology, *J. Geophys. Res., 99*, 21,983- 22,000, 1994.

Rice, J. R., The mechanics of Earthquake rupture, in *Physics of the Earth's Interior*, pp. 555-649, North-Holland, New York, 1980.

Rice, J. R., Spatiotemporal complexity of slip on a fault, *J. Geophys. Res., 98*, 9885-9907, 1993.

Robinson, R., and R. Benites, Synthetic seismicity models of multiple interacting faults, *J. Geophys. Res., 100*, 18,229-18,238, 1995.

Rockwell, T. K., S. Lindvall, M. Herzberg, D. Murbach, T. Dawson, and G. Berger, Paleoseismology of the Johnson Valley, Kickcapoo and Homestead Valley faults of the Eastern California Shear Zone, *Bull. Seismol. Soc. Am.*, 90, 1200-1236, 2000.

Savage, J. C., Dislocations in seismology, in: *Dislocations in Solids*, vol. 3, edited by F.R.N. Nabarro, pp. 251-339, North-Holland, New York, 1980.

Savage, J. C., Equivalent strike-slip earthquake cycles in half-space and lithosphere-asthenosphere Earth models, *J. Geophys. Res., 95*, 4873-4879, 1990.

Savage, J. C., and J. L. Svarc, Postseismic deformation associated with the 1992 M_W=7.3 Landers earthquake, southern California, *J.Geophys. Res., 102*, 7565-7577, 1997.

Savage, J. C., J. D. Byerlee, and D. A. Lockner, Is internal friction friction?, *Geophys. Res. Lett., 23*, 487-490, 1996.

Scholz, C. H., N. H. Dawers, J.-Z. Yu, M. H. Anders, and P. A. Cowie, Fault growth and fault scaling laws: Preliminary results, *J. Geophys. Res., 98*, 21,951-21,961, 1993.

Shibazaki, B., and M. Matsu'ura, Spontaneous processes for nucleation, dynamic propagation, and stop of earthquake rupture, *Geophys. Res. Lett., 19*, 1189-1192, 1992.

Sibson, R. H., Fault zone models, heat flow, and the depth distribution of earthquakes in the continental crust of the United States, *Bull. Sesmol. Soc. Am., 72*, 151-163, 1982.

Simpson, R. W., and P. A. Reasenberg, Earthquake-induced static stress changes on central California faults, in *the Loma Prieta, California Earthquake of October 17, 1989 Tectonic Processes and Models*, edited by R. W. Simpson, *U.S. Geol. Surv. Prof. Pap., 1550-F, 55-89, 1994.*

Sornette, D., P. Miltenberger, and C. Vanneste, Statistical physics of fault patterns self-organized by repeated earthquakes, *Pure Appl. Geophys., 142*, 491-527, 1994.

Stein, R. S., G. King and J. Lin, Stress triggering of the 1994 *M*-6.7 Northridge, California, earthquake by its predecessors, *Science, 265*, 1432-1435, 1994.

Stein, R. S., A. A. Barka, and J. H. Dieterich, Progressive failure on the North Anatolian fault since 1939 by earthquake stress triggering, *Geophys. J. Int., 128*, 594-604, 1997.

Stirling, M. W., S. G. Wesnousky, and K. Shimazaki, Fault trace complexity, cumulative slip, and the shape of the magnitude-frequency distribution for strike-slip faults: A global survey, *Geophys. J. Int., 124*, 833-868, 1996.

Thatcher, W., Nonlinear strain build-up and earthquake cycle on the San Andreas Fault, *J. Geophys. Res.*, *88*, 5893-5902, 1983.

Wallace, R. E., Grouping and migration of surface faulting and variations in slip rates on faults in the Great Basin Province, *Bull. Seismol. Soc. Am.*, *77*, 868-876, 1987.

Ward, S., A synthetic seismicity model for southern California: Cycles, probabilities, hazard, *J. Geophys. Res.*, *101*, 22,393-22,418, 1996.

Wdowinski, S., and R. J. O'Connell, On the choice of boundary conditions in continuum models of continental deformation, *Geophys. Res. Lett.*, *17*, 2413-2416, 1990.

Wesnousky, S. G., The Gutenberg-Richter or characteristic earthquake distribution, which is it?, *Bull. Seismol. Soc. Am.*, *84*, 1940-1959, 1994.

Zhao, D., H. Kanamori, and D. Wiens, State of stress before and after the 1994 Northridge earthquake, *Geophys. Res. Lett.*, *24*, 519-522, 1997.

Zoback, M., and G. C. Beroza, Evidence for near-frictionless faulting in the 1989 (M=6.9) Loma-Prieta, California, earthquake and its aftershocks, *Geology*, *21*, 181-185, 1993.

A. Agnon and V. Lyakhovsky, Institute of Earth Sciences, Hebrew University, Givat Ram, Jerusalem 91904, Israel. (vladi@cc.huji.ac.il)

Y. Ben-Zion, Department of Earth Sciences, University of Southern California, Los Angeles, CA 90089-0740. (benzion@topaz.usc.edu)

(Received October 19, 1999; revised April 6, 2000; accepted June 12, 2000.)